HHS Public Access

Author manuscript

IEEE Sens J. Author manuscript; available in PMC 2022 September 15.

Published in final edited form as:

IEEE Sens J. 2021 September 15; 21(18): 19647–19661. doi:10.1109/jsen.2021.3094092.

Metal-organic Framework Materials Coupled to Optical Fibers for Chemical Sensing: A Review

Chen Zhu [Member, IEEE], **Rex E. Gerald II**, **Jie Huang [Senior Member, IEEE]**

Department of Electrical and Computer Engineering, Missouri University of Science and Technology, Rolla, MO 65409, USA.

Abstract

Metal-organic frameworks (MOFs), a newer class of crystalline nanoporous materials, have been in the limelight owing to their exceptional tunability for structures and physicochemical properties, and have found successful applications in gas storage, gas separation, and catalysis. The mesmerizing properties of MOFs, especially the extensive and tunable porosity and chemical selectivity, also make them an excellent candidate class as chemo-sensory materials. Moreover, MOF-based sensors have attracted considerable attention in the past decade. Recent literature reviews focused on the progress of MOF-based electronic sensors and luminescent MOF sensors, while sensors exploiting the dielectric properties (refractive index) of MOFs were also demonstrated and discussed very recently. The motivation of this report is to provide, for the first time, a general review on such MOF sensors with a particular focus on miniature optical fiber (OF) based MOF sensors and to demonstrate the promising potential of MOFs as dielectric coatings on OF for highly sensitive chemical sensing. The fundamental principle of OF-MOF sensors relies on the tunability of the refractive index of a MOF, which is dependent on the amount and type of adsorbed guest molecules in the MOF pores. MOF sensors based on different optical sensing principles are reviewed; challenges and perspectives on further research into the field of OF-MOF sensors are also discussed.

Index Terms—

Sensors; metal-organic frameworks; fibers; optical fiber sensors; thin films; gases; adsorption

I. Introduction

METAL-ORGANIC frameworks (MOFs) are a newer class of crystalline nanoporous materials that have witnessed a meteoric growth in the last several decades [1]–[4]. MOFs are formed by the coordination of inorganic metal nodes (ions or clusters) and organic ligands. The variety of metal ions or clusters, organic ligands, and how the metal nodes are joined with the organic ligands affords virtually limitless combinations and thereby provides MOFs with additional advantages over traditional porous materials (e.g., zeolite), including an unparalleled degree of tunability and structural diversity, and tailorable chemical and physical properties [1]. The large internal surface areas and permanent porosity of MOFs

(Corresponding authors: Chen Zhu and Jie Huang, cznwq@mst.edu, jieh@mst.edu).

facilitate the extensive adsorption of guest molecules with enhanced host-guest interactions. The additional high-degree tunability of the size, shape, chemical composition, and surface environment of the open pores in MOFs can potentially lead to selective sequestering of specific guest molecules. As a result, the applications of MOFs in various applications, such as gas storage, gas separation, and heterogeneous catalysis, have proliferated in the past years [2], [5], [6]. The exploration of MOFs as chemo-sensory materials started only recently, yet tremendous advancements were achieved in the last decade [1], [7]–[9]. The unique features of MOFs make them a superior candidate over other classes of chemosensing materials.

In comparison with conventional chemo-sensory materials such as metal oxides, which require high operating temperatures and are deficient in selectivity, MOFs have many advantages such as large surface area, extensive porosity with highly tunable size and shape features, fast response time, room-temperature operation capability, high selectivity, and reliable reversibility and repeatability metrics. The foundation of MOF materials for chemical sensing relies on their permanently microporous structure. In traditional chemical sensors based on less porous or non-porous materials such as metal oxides and polymers, an additional pre-concentration process employing a porous adsorbent as the analyte concentrator is typically required for sensitivity enhancement [10]. The pre-concentration process can be effectively and efficiently circumvented by utilizing nanoporous MOFs as chemosensory materials due to their inherently extensive porosity, where the porous frameworks of MOFs can serve as chemical hosts for concentrating guest molecules (i.e., the target analyte) [7]. However, the unit cell size of the open pores inside MOFs is typically in the angstrom to nanometer range, making it challenging to directly measure the response from an individual pore within the MOF. Therefore, one major challenge in the development and implementation of MOFs as chemo-sensory materials is the signal transduction from MOF sensing layers. The most promising means of utilizing MOFs for chemical detection is to adopt a macroscopic perspective, whereby changes in the MOF material on exposure to a target analyte as a whole are measured. Notionally, any changes in the physicochemical properties of the MOF material in response to the variations of the target analyte can be considered as a sensing signal and can be interpreted using proper signal transduction schemes.

To date, a variety of MOF-based chemical sensors that operate based on different signal transduction schemes were reported and categorized, as schematically illustrated in Fig. 1. The MOF chemical sensors are categorized by the principle of how the MOF responds to the guest analyte. Adsorption of guest molecules inside the MOF open pores results in changes in the electrical, mechanical, optical, or dielectric properties of the MOF materials, and these changes, as well as the magnitudes of these changes, are exploited as measures for qualitatively and quantitatively detecting guest (target) analytes. Large numbers of reported MOF chemical sensors are based on the luminescence property of MOF materials [8], where the MOF not only recognizes the target molecules but also produces an optical signal that can be quantified. Another type of MOF sensor relying on the optical properties of MOFs is directly based on the color change in the MOF upon loading of guest molecules, so-called vapochromism [11]. However, most MOFs are not luminescent and do not exhibit the behavior of color change. Therefore, the

optical signal transduction is not a generalizable approach for developing MOF chemical sensors. Inspired by the traditional organic polymers and zeolite-based chemical sensors, electromechanical MOF devices based on the quartz crystal microbalance (QCM), the surface acoustic wave (SAW), and the microcantilever (MCL) were developed for chemical sensing [12]–[14], exploiting the sorption induced gravimetric changes of the integrated MOF layer. Gravimetric-based MOF sensors employ a thin film of MOF that is coated on the surface of an electromechanical device, which selectively adsorbs an analyte of interest and detects the mass change with nanogram sensitivity. Changes in mass of the MOF film caused by adsorption of guest molecules in its pores modify the frequency of a resonant vibration propagating perpendicular to the surface of a quartz crystal (QCM), the frequency of an acoustic wave traveling parallel to the surface (SAW), or the oscillation frequency/degree of bending of a microcantilever (MCL), and induced mechanical signals can be detected and quantified. In these sensors, the physical interface between the MOF and the device surface must be tight and strong to obtain satisfactory measurement sensitivity. The morphology of the MOF might also contribute to the sensitivity of these devices. More electromechanical MOF sensors are expected to be developed as the MOF film coating methods keep evolving and advancing [1]. Since its first report in 2009 [15], electronic MOF sensors have attracted great research interest, thanks to their low cost and ease of sensor fabrication and interrogation. The electronic MOF sensors take advantage of the dependence of the electrical properties of MOFs, including the impedance, capacitance, resistance, and work function, on the interaction between the MOF and a target analyte. Details about recent progress on electronic MOF sensors can be found in recent reviews [7], [9]. The bottleneck for developing electronic MOF sensors is that most of the reported MOFs are not electrically conductive. It is envisioned that a new generation of simple, reliable, and room-temperature chemiresistive MOF sensors will subsequently emerge as highly conductive MOFs are successfully developed.

Another type of bulk property of MOFs that has been employed for sensing is the dielectric property. The dielectric constant is a measure of the interactions of electromagnetic (EM) waves with polarizable matter, depending on the number of polarizable electrons as well as the polarizability of the electrons. The dielectric properties of a MOF, e.g., the dielectric constants (or refractive indices, RI in the optical domain), are dependent on the MOFs and the numbers and types of guest molecules that are adsorbed inside the MOF pores. As the MOF adsorbs polarizable molecules from the ambient environment, the guest molecules displace vacuum in the open pores of the MOF and therefore increase the effective refractive index of the guest-host MOF system. Therefore, combining the chemically specific adsorption of MOF materials with the high sensitivity of EM dielectric spectroscopy (e.g., low-profile EM waveguide dielectric sensors) seems to provide a universal strategy for developing a new generation of chemical sensors. As a MOF host adsorbs target analyte guests from the ambient environment, its dielectric properties vary, resulting in changes in the EM wave-matter interactions. The changes in the EM wave-matter interactions cause the characteristic spectrum derived from the EM dielectric sensor device to shift with respect to frequency and/or power, from which adsorption of the guest molecules can be accurately detected and quantified in real-time.

In this paper, a general review of MOF chemical sensors that exploit the dielectric properties of MOFs upon interactions with target analytes is presented with a special focus on optical fiber-MOF (OF-MOF) sensors. The next section reviews the reported OF-MOF sensors from the literature, categorized by the optical sensing principle. A few examples of microwave dielectric spectroscopy-based MOF sensors are also presented and compared with the OF-MOF sensors. Challenges and perspectives on further research in the OF-MOF sensor arena are also discussed. It is worth noting that although optical fiber sensing has experienced tremendous growth and advancements in the past four decades, the MOF-based optical fiber sensing technology is still in its infancy.

II. Review of OF-MOF Sensors

Originally developed for low-loss and long-haul telecommunication applications, OFs have been extensively explored in the sensing field. OF sensors have been widely and successfully used in an expansive range of sensing applications, such as structural health monitoring, down-hole monitoring, environmental monitoring, and chemical and biological sensing [17]–[20]. Among various OF sensors, OF RI sensors have attracted great interest for chemical sensing, thanks to their prominent features over traditional electrical sensors, such as compact size, high sensitivity, immunity to EM interference, remote operation, and capabilities for multiplexing and distributed sensing. The fundamental principle of OF RI sensors relies on the light-matter interaction, where changes in the RI of the surrounding medium of an OF lead to changes in the properties in the guided light in the OF, e.g., through its evanescent field. These light properties include intensity, wavelength, phase, and polarization. However, one of the major challenges for using OF RI sensors for chemical sensing is the lack of chemical specificity. Another limiting aspect of OF RI sensors for chemical sensing, for example for gas sensing, is that the changes in the RI caused by variations of gas concentrations are extremely small, making them challenging to directly measure. Therefore, with the emergence of MOF materials that possess extensive porosity and potentially molecular-level chemical selectivity, it is promising to develop OF-MOF sensors that combine the advantages of OF sensors and MOFs. The MOFs selectively adsorb the target molecules and increase the local concentration of the analyte in the MOF, due to their large surface area, which consequently amplifies the changes in the RI induced by variations of the gas analyte concentration. The advancement in MOF thin film coating methods makes it possible to directly grow a thin film of a MOF on the surface of an OF with controlled film thickness and morphology, further facilitating the development of OF-MOF chemical sensors. This section reviews the existing OF-MOF sensors, categorized based on the optical sensing principle, including interferometry, evanescent field sensing (e.g., long-period gratings-based), transmission spectroscopy, and (localized) surface plasmon resonance. Each of the OF-MOF sensors has its own strengths; for example, interferometric sensors are simple to fabricate and are miniature in size; long-period gratings are well known for their high sensitivity; the cost of an interrogation unit for a transmission spectroscopy-based sensor device (e.g., an etched OF) is very low, and MOF thin films can be easily integrated in such a device. Note that a few fluorescence-based OF-MOF sensors were also reported, where the OFs were used as portable and high-efficiency

waveguides to probe the fluorescent properties of the sensing MOF materials [21]–[23]. Details about the fluorescence-based sensors will not be covered in this review.

A. Interferometry

Fiber optic interferometry is one of the most widely used sensing approaches due to its high sensitivity. Different interferometric configurations, such as the Michelson interferometer (MI), the Mach-Zehnder interferometer (MZI), the Sagnac interferometer (SI), and the Fabry-Perot interferometer (FPI), have been demonstrated for the measurement of a variety of physical and chemical quantities [24]. The fundamental principle of an interferometer for sensing applications relies on correlating the parameter of interest (e.g., concentration of a gas analyte) to the phase delay of the interferometer. Among different configurations, the FPI is especially attractive due to its simple structure, ease of fabrication, small size, and reflection-based measurement. An FPI consists of two partial reflectors separated by a certain distance (e.g., tens to hundreds of μm), where an FP etalon is formed between the two reflectors. The incident light comes in the FP etalon and experiences multiple internal reflections in the cavity. As a result, an interference pattern is generated due to the superposition of the reflected light beams by the two reflectors. The striking feature is that a chemically functional thin film (e.g., a thin layer of MOF) can be directly deposited onto the cleaved endface of an OF to form a low-finesses FP etalon, as schematically illustrated in Fig. 2. The fiber-MOF interface serves as the first reflector and the MOF-ambient interface (e.g., MOF-air interface) functions as the second reflector, both interfaces/reflectors forming the FP cavity. Due to the low reflectivity of the two reflectors (ca. < 4%), the FPI can be modeled by a simple two-beam interference equation, and the total intensity of the reflection spectrum (i.e., the interference pattern) can be expressed as

$$I = I_1 + I_2 + 2\sqrt{I_1 I_2}\cos\left(\frac{4\pi nd}{\lambda} + \varphi\right) \tag{1}$$

where I_1 and I_2 denote the reflected light intensities by the first reflector and the second reflector of the MOF FP cavity, respectively; λ is the optical wavelength of the input probing light; n is the effective RI of the MOF-guest material; d is the thickness of the MOF layer; and, ϕ represents the initial phase of the interferometer (a constant). When the phase term in eq. (1) satisfies the interferometer phase-matching condition, where the intensity reaches a series of minima, a destructive interference pattern results, manifesting as a series of dips; one such dip is shown in Fig. 2(b). The wavelengths of the series of dips can be predicted by

$$\lambda_m = \frac{4\pi nd}{(2m+1)\pi - \varphi}, \quad m = 0, 1, 2, \ldots \tag{2}$$

where m is a non-negative integer denoting the resonance order of the dip wavelength. And, the optical thickness of the MOF layer, defined by the product of the effective RI and the physical thickness, can be calculated based on

$$nd = \lambda_m \frac{(2m+1)\pi - \varphi}{4\pi}, \quad m = 0, 1, 2, \ldots \tag{3}$$

As mentioned above, the key here to employing a MOF for chemical sensing is the tunability of its effective RI. Due to its inherent porosity, the effective RI of a MOF depends on the adsorbed guest molecules and is a volume-weighted average of the indices of the open cavity (i.e., vacuum with RI of 1), filled cavity (i.e., the guest molecule with RI > 1), and the framework [25]. As the guest uptake occurs, the guest molecules will replace vacuum in the open pores, thereby increasing the overall effective RI of the MOF. The increase of the effective RI will consequently increase the optical thickness of the MOF layer and cause the redshift of the dip wavelength, as illustrated in Fig. 2(b). The relationship between the shift of the dip wavelength ($\Delta\lambda_m$) and the change in the effective RI (Δn) can be obtained by differentiating eq. (2), and can be expressed by

$$\frac{\Delta\ \lambda_m}{\lambda_m} = \frac{\Delta\ n}{n} \tag{4}$$

Thus, the shift in the corresponding dip wavelength is proportional to the change in the effective RI of the MOF layer caused by the adsorption of guest molecules. In turn, by tracking the wavelength shift, the guest-host interaction can be monitored in real-time, indicating that the temporal process (e.g., the adsorption curve) can be detected at any time. The described process transforms a tip of an OF, deposited with a MOF layer, into a miniature chemical sensor device with high sensitivity and a small footprint. For the FPI-based OF-MOF sensor, the MOF layer serves three functions: sensing cavity, receptor, and analyte concentrator. That is, it forms the FP cavity that can detect changes in RI; it recognizes the target analyte molecules; and, it concentrates the target molecules due to its large internal surface area. It is worth mentioning that the shift in the dip wavelength can be typically resolved to 10 pm, so the resolution of the FPI and other interferometers for RI sensing can reach 10 ppm, given that the dip wavelength and the initial RI to be 1550 nm and 1.5, respectively.

The first FPI-based MOF sensor device was reported in 2010, which was fabricated by depositing thin films of ZIF-8 on glass or silicon slides and worked in the UV-vis region [25]. Thin films of ZIF-8 (50 nm) were obtained by directly immersing the substrate slides in a freshly prepared methanolic solution at room temperature for approximately 30 min, and thicker films could be obtained by repeating the process with fresh solutions through layer-by-layer assembly, with a reproducible growth rate of ca. 100 nm per cycle. A porotype device based on a glass slide ($10 \times 10\ mm^2$) with a 1000 nm-thick ZIF-8 film was fabricated and exposed to various concentrations of propane, showing rapid (1 min) and reversible responses. The selectivity and hydrophobicity of the ZIF-8-based FP device were also verified. Note that based on the spectral shift of the device in response to the analyte, the volume fraction of the analyte in the framework of the MOF could also be estimated. The glass side-based MOF FP device demonstrated the feasibility of using interferometry to interrogate MOF thin films for highly sensitive chemical sensing and paved the way to develop miniature OF-based MOF FP devices.

In 2016, the first OF-based MOF FP device was reported, where a thin film of water-stable MOF (UiO-66) was coated on the endface of an optical fiber for detection of Rhodamine-B

(RhB) concentrations in aqueous environments [26], [27]. A cleaved standard single-mode fiber (SMF-28) with a section of polymer coating removed was first coated with a plasma polymer film using a custom-built radio frequency glow discharge plasma polymerization reactor. The pre-treated OF was then placed in a precursor solution of UiO-66, and the solution was heated at 120°C for 24 h. Fig. 3 shows the scanning electron microscope (SEM) images of the samples. The thickness of the UiO-66 thin film coated on the fiber endface was estimated to be 17–22 μm, composed of a total of 10–12 layers. Fig. 4 presents the experimental results of the UiO-66 MOF-coated OF tip device designed for the detection of RhB in water. The device was interrogated using a broadband light source and a bulky optical spectrum analyzer (OSA). The measured interference patterns of the device when immersed in different concentrations of RhB/water are plotted in the inset of Fig. 4. The spectral valley (i.e., the dip wavelength) shifted to longer wavelength with increasing RhB concentrations. Note that the tracked spectral valley moved out from the observation wavelength window at a concentration of 15 mM, and a lower-order valley emerged in the observation window. Fig. 4 shows the calculated optical thickness of the MOF film as a function of RhB concentration in DI water. The higher the concentration, the more uptake of RhB molecules in the active sites of the MOF at equilibrium before saturation, and therefore the larger the optical thickness. Although it turned out the adsorption of RhB molecules was irreversible, the proposed device could be used for long-term monitoring of RhB in water, with a detection limit of 48 ppm (0.1 mM). Note that the thickness of the MOF film must be at least in the μm range to obtain multiple periods of the interference fringes (in the form of sinusoidal functions) from the FPI device using a cost-effective light source with a bandwidth of 100 nm. However, depositing such a thick layer of MOF on the endface of an OF is relatively challenging and time-consuming. Also, the interrogation unit including an OSA was bulky and expensive. To overcome the limitations of a bulky apparatus, ultra-compact OF-MOF sensors based on FP nanocavities were proposed [28]. Thin films of ZIF-8 with thicknesses in the hundreds of nm range were deposited onto the cleaved enface of OFs at room temperature. A differential power interrogation method based on a cost-effective data acquisition unit was used to interrogate a pair of OF-MOF FP devices, as illustrated in Fig. 5. By carefully choosing the thicknesses of the MOF films in the two devices, the differential interrogation not only was cost-effective, but also increased the sensitivity of the system and eliminated the potential signal drift that can be caused by the power fluctuations of the light source. The size of the paired sensors was only 157 μm^2, and the resolution reached 0.019 CO_2 vol%. Additionally, due to the small thicknesses of the MOF films, the response and recovery times for the two-FP sensor device were only 141 ms and 310 ms, respectively. The simple room-temperature coating method and the low-cost interrogation unit used for the dual FP nanocavities-based OF-MOF sensor make batch-fabrication possible and facilitate the production of an overall inexpensive sensor system.

Apart from thin films, other morphologies of MOF materials can also be used to construct FPI-based OF-MOF sensors, such as single crystal and thin bed motifs, which can be physically attached to the endfaces of OFs to form FP sensor devices. Although the response rate of single crystal- or thin bed-based sensors may pose limitations due to the larger MOF size samples compared to thin films (i.e., decreased rate of guest diffusion within

the pores), single crystal- or thin bed-based sensors provide unique features, such as ease of sensor fabrication, sensor longevity, and high stability. A detailed comparison of the three different morphologies of MOF materials as sensors can be found in [29]. A MOF single crystal-based OF-MOF-FP sensor was reported by physically attaching a MOF single crystal (HKUST-1, ~70 μm in thickness) to the endface of an OF with the assistance of a thin layer of adhesive [30], as shown in Fig. 6(a). In addition to quantification of loading of the target analyte, the time profile of the uptake process was measured based on analyzing the shifts of the interference patterns obtained from a prototype sensor device in real-time, as shown in Fig. 6(b). The inset in Fig. 6(b) shows the time derivative of the changes in the RI with respect to time. The oscillations in the time derivative plot, revealing the oscillations of the uptake rate during the equilibrating uptake period, were not fully understood and require further investigation. Importantly, the MOF single crystal-based sensor motif provides a route to use finely-controlled polarized light to probe the occupancy and spatial distribution of guest molecules inside the MOF pores, taking advantage of the light-guiding and confinement capabilities of OF and the fact that the site distribution of guest molecules in the MOF is highly anisotropic [31].

In addition to FPI sensors, MZI-based OF-MOF sensors were also developed. A μm-level thin film of graphene oxidenickel (GO-Ni) MOF was coated on the cylindrical surface of an OF-based MZI interferometer [32]. The MZI was simply fabricated by splicing a section of a single-mode fiber between two single-mode fibers using the core-offset fusion procedure. The as-formed core-offset structure is well known for its capability for RI sensing. The GO-Ni MOF coated OF-MZI was tested for hydrogen sensing, showing good adsorption ability up to 1 wt% concentration at 18°C and atmospheric pressure. Another widely used OF refractometer, the single-mode no-core single-mode (SNS) fiber structure was also employed as a sensing platform and was coated with a thin film of ZIF-8 for highly specific sensing applications [33]. The ZIF-8 film was embedded with urease (an enzyme that catalyzes the hydrolysis of urea), and the resultant ZIF-8/urease film was used to detect urea. The no-core fiber was tapered to further increase the RI sensitivity of the SNS structure by 26 times; the ZIF-8/urease film was coated on the tapered section of the structure. An overview of the experimental setup and performance of the SNS biosensor is shown in Fig. 7(a) and (b), respectively. The SNS sensor coated with ZIF-8/urease exhibited a sensitivity of 0.8 nm/nM, a higher sensitivity compared to the reference sensors with free ZIF-8 and free urease. This work demonstrated a simple strategy to develop OF-MOF biosensors and paved the way to couple different MOFs and enzymes for highly sensitive biosensing applications.

B. Evanescent Field Sensing (Long Period Gratings-Based)

One of the most well-known OF RI sensors is the long period grating (LPG) owing to its ultra-high sensitivity to its surrounding environment. An LPG consists of a periodic modulation of the RI of the core of a single-mode fiber with a pitch size of hundreds of μm and a total length in the cm range. An LPG is schematically illustrated in Fig. 8(a). The periodic RI modulation couples the propagating fundamental core mode to a set of co-propagating cladding modes, producing a series of attenuation bands at discrete wavelengths (so-called resonant wavelengths) in the transmission spectrum. Each of the attenuation bands

is a result of the coupling between the core mode and a specific cladding mode, and each of them exhibits different sensitivities to environmental changes. Generally, the longer the resonant wavelength and the higher order of the cladding mode, the higher the RI sensitivity. The *m*-order resonant wavelength can be calculated by equating it to the phase-matching condition:

$$\lambda_m = \left(n_{core} - n_{cladding(m)}\right) \Lambda \tag{5}$$

where n_{core} is the effective RI of the core mode; $n_{claddingg(m)}$ is the effective RI of the LP_{0m} cladding mode; and, represents the period of the LPG, i.e., the pitch length. As the RI of the surrounding medium changes, the effective RI of the cladding modes changes, leading to a shift in the corresponding resonant wavelength, as illustrated in Fig. 8(b).

A unique feature of LPGs is that the phase-matching condition for each of the high-order cladding modes contains a turn-around-point (TAP, also named turning point), where the highest RI sensitivity is achieved, i.e., TAP-LPG. The TAP can be realized by carefully choosing the pitch of the LPG. The TAP refers to a specific point on the dispersion curve of a cladding mode of an LPG at which two resonant wavelengths coincide with each other [35]. The transmission power and bandwidth of the resultant U-shaped attenuation band of a TAP-LPG strongly depend on the surrounding media, providing an ultra-sensitive chemical sensing platform with ppm-level RI resolution. When an increase in the surrounding RI is large, the LPG deviates the TAP, and the U-shaped attenuation band splits into two resonant dips. Therefore, the separation between the two resonant dips can also be used as a reference for RI sensing. When modified with appropriate chemically/biologically functional coatings (e.g., a MOF thin film), as shown in Fig. 8(c), the transmission spectrum of the LPG is determined by the effective RI of the coatings, which are dependent on the concentrations of target chemicals or biological analytes [36], [37].

An OF LPG coated with a thin film of ZIF-8 was reported for the detection of organic vapors in 2015 [38]. Different thicknesses of ZIF-8 films were directly deposited on the cylindrical surface of OF LPGs through a simple and cost-effective in-situ crystallization and layer-by-layer assembly approach, the same strategy reported in [25]. The film deposition process was monitored in real-time by tracking the central wavelength separation of the LP_{019} cladding mode. Fig. 9(a) shows the measured transmission spectra of an LPG after the deposition of the 1st through the 5th growth cycle of ZIF-8 thin films on its surface (growth rate: ca. 50 nm/growth cycle). The continuous dynamic response of the LPG is presented in Fig. 9(b). As the LPG was immersed in the prepared solution, the wavelength difference drastically increased due to the fact that the surrounding medium of the LPG changed from air to the solution (the solution had a much larger RI than air). Following the step change, a continuous increase in the wavelength difference was observed, as indicated in the highlighted region. The continuous increases were a result of in-situ crystallization of ZIF-8 on the LPG. The black lines in Fig. 9(b) indicated that the wavelength difference increased as thicker films of ZIF-8 were deposited on the fiber. LPGs with different ZIF-8 thicknesses were exposed to methanol, ethanol, 2-propanol, and acetone vapors, and the LPGs showed specific responses to methanol. Penetrations of the organic guest molecules such as methanol into the pores of the ZIF8 film resulted in increases in the

effective RI of the film, which were quantified by tracking the wavelength separation. The LPG with five growth cycles (ca. 250-nm film thickness) exhibited the highest sensitivity to methanol concentrations ranging from 1790 to 27,900 ppm, with a limit of detection (LoD) of 1454 ppm. Although the obtained LoD was too high for real-world applications, the results demonstrated the feasibility of combining an LPG with a MOF material for selective chemical sensing. Later, Hromadka et al. optimized the pitch of the LPG to operate at the TAP to increase the sensitivity. An LPG with a grating period of 109.5 μm and a length of 30 mm was deposited with a ZIF-8 film using five growth cycles, and the modified LPG operated precisely at the TAP [39–41]. The responses of the LPG to various concentrations of acetone and ethanol vapors were investigated by tracking the bandwidth of the U-shaped attenuation band, showing drastically improved LoDs of 6.67 and 5.56 ppm, respectively. Figs. 10 includes examples of the transmission spectra of an LPG when exposed to different concentrations of ethanol. Hromadka et al. also deposited HKUST-1 thin films with different thicknesses (10 nm, 20 nm, and 55 nm) onto the surface of LPGs, using in-situ crystallization and layer-by-layer techniques, for the detection of carbon dioxide [42], [43]. The results revealed that the 50 nm HKUST-1 coated LPG exhibited the highest sensitivity to CO_2 observed in their work, in the range of 500 ppm to 40,000 ppm. The LPG was not operating at the TAP, and the LoD was estimated to be 401 ppm. In addition to gas sensing, a label-free LPG biosensor based on a thin film of ZIF-8, with encapsulated glucose oxidase (GOx), was also reported [44]. The ZIF-8 material acted as both a protective shell for GOx and an analyte collector. The resultant ZIF-8/GOx composite film showed high protein encapsulation efficiency and high stability under harsh conditions. An LPG coated with the composite film exhibited a linear response (0.5 nm/mM, wavelength shift/concentration) to various concentrations of glucose solutions in the range 1–8 mM.

In addition to direct sensing, a pair of LPGs were employed as a cladding mode exciter and a combiner to form a fiber in-line MZI. The composite LPG sensor device was used for studying light-matter interactions in a ZIF-8 thin film that was coated on the fiber over a length of ~10 cm [45]. Changes in the effective RI of the 300nm-thick ZIF-8 film caused by exposure to methanol and ethanol were precisely calculated based on the magnitudes of the shifts of the interferograms derived from the MZI. The LoD of the MZI-based OF-MOF sensor for ethanol vapor sensing was estimated to be lower than 9.8 ppm, and the response was quite linear as the concentration increased from 9.8 ppm to 540 ppm.

C. Transmission Spectroscopy

Light is strictly confined in the core of an OF based on the concept of total internal reflection so that light can propagate along the OF for a long distance with low loss. However, when an OF is used for sensing, it is preferable to enhance the light-matter interaction to increase the measurement sensitivity. One of the simplest approaches to improve the evanescent field of an OF is to partially or completely remove the cladding of the OF, where the cladding-reduced section affords a drastically enhanced evanescent field, which can directly interact with the surrounding medium. Changes in the optical properties of the surrounding medium, e.g., RI or spectral adsorption, lead to modulation of the light propagating in the OF due to the intense evanescent field-matter interaction, making possible

evanescent field spectroscopy [46]. Deposition of chemically functional thin films (e.g., zeolite) onto the cladding-reduced section of an OF provides a unique route to develop simple and highly sensitive OF chemical sensors [47].

To this end, an OF-MOF chemical sensor was developed based on an etched multimode fiber (diameter of core/cladding: 105/125 μm) with a ZIF-8 thin film coating [16]. The sensor characterization system with an enlarged view of the sensor is illustrated in Fig. 11(a). SEM images of the ZIF-8 coated OF are shown in Figs. 11(b) and (c). A standard multimode fiber was first etched using hydrofluoric acid for 50 min, followed by the in-situ crystallization and layer-by-layer assembly processes, where thin films of ZIF-8 with a desired thickness, e.g., 200 nm, could be obtained. Adsorption of gas molecules in the ZIF-8 layer resulted in small changes in RI of the ZIF-8 layer, leading to changes in the transmission spectrum of the sensor. Measurements were performed at ~242 nm because a strong absorption band caused by the 2-mIM linker within the ZIF-8 falls at 242 nm. Dynamic responses of a prototype sensor, with a 350 nm-thick ZIF-8 coating, to different gases such as H_2, CO, O_2, and CO_2 were tested, as shown in Fig. 11 (d). The OF-MOF sensor exhibited the largest sensitivity to CO_2 because the ZIF-8 layer had the largest adsorption selectivity for CO_2 among the test gases. The sensitivity was expected to be further increased by increasing the sensing length of the sensor. The reversibility and response times of different prototype sensors were also investigated, showing that the sensor with a thinner thickness of ZIF-8 (i.e., 200 nm) had fast response and recovery times of 9 and 14 s, respectively. The cross-sensitivity of the sensor to humidity and temperature was not investigated. Nevertheless, the results revealed that etched OFs could become a simple and highly sensitive platform for developing chemical sensors based on thin films (e.g., hundreds of nm) of MOF materials. The same author later reported a strategy involving the deposition of a hydrophobic layer of alkylamine (i.e., oleylamine) on a Co/ZIF-8 film to enhance the stability of the MOF in responses to various concentrations of dry/wet CO_2 with unaltered porosity [48]. The alkylamine modified MOF films with improved CO_2/H_2O selectivity together with the etched OF sensing platform paved the way to develop more practical chemical sensors with improved stability.

In addition to UV transmission spectroscopy, OF-MOF sensors based on near-infrared (NIR) adsorption were also reported [49]–[51]. The principle of infrared absorption spectroscopy is described by the Beer-Lambert Law [51]

$$I = I_0 \exp(-\gamma \alpha L) \tag{6}$$

where I and I_0 denote the transmitted and incident light intensity; α represents the adsorption coefficient of the gas, which is wavelength dependent and also relies on the gas concentration; γ is the enhancement factor ($\gamma = 1$ for free-space gas cells), and is <1 for evanescent field OF sensors, moreover, the stronger the evanescent field, the larger the enhancement factor; and, L is the sensing length. Traditional NIR gas sensors suffer from low detection sensitivity because most gases do not have fundamental vibration bands in the NIR region. Therefore, to improve the sensitivity, OF-based NIR gas sensors typically have a sensing length of several meters. Taking advantage of the extensive porosity and large surface area, MOFs can be coated on OF NIR sensors as a gas concentrator to enhance

the evanescent field-matter interaction and thereby increase the enhancement factor γ, and consequently the sensitivity. An etched multimode fiber with a core diameter of 75 μm and length of 8 cm, coated with a 100 nm-thick Cu-BTC film, was employed for CO_2 sensing [50]. Since the absorption band of CO_2 falls in the wavelength range 1565–1585 nm and the Cu-BTC does not show significant adsorption in the same narrow window, the responses of the sensor were measured at 1572.5 nm, revealing rapid responses (< tens of seconds) and an LoD of 500 ppm. The reported sensor came to be the shortest OF NIR sensor for CO_2 detection in the 1.57-μm region. Later, the authors performed a more comprehensive study on the NIR-based OF-MOF sensor, where an etched single-mode fiber with a length of only 5 cm was coated with a 100 nm-thick Cu-BTC film for detection of CO_2 [51]. The NIR absorption spectra of CO_2 measured using the Cu-BTC-coated OF and a reference quartz gas cell are shown in Fig. 12(a) and (b), respectively. Interestingly, the rotational fine lines disappeared in the spectrum obtained from the OF-MOF device, which is due to the condensed phase of the CO_2 molecules inside the MOF pores. However, the broad peaks in the spectrum matched well with some of the general features shown in the reference spectrum (Fig. 12(b)), especially the envelope of peaks in the range 1568–1572 nm. The responses of the sensor to various concentrations of CO_2 with Ar as the carrier gas were investigated, showing an LoD of as low as 20 ppm. The response and recovery times of the sensor were also studied, and the results showed that the response and recovery times increased significantly from 10/12s to 106/530s as the gas under test changed from pure CO_2 to 30 ppm CO_2. The time increases were explained by different sorption and desorption kinetics at high and low concentrations, evolving from physisorption to chemisorption. Influences of interference gases such as N_2 and water vapor on the sensor's response were also examined.

An OF-MOF sensor requires a physical interface between the MOF and the OF sensing platform, which is typically accomplished by directly growing a thin film on the OF, involving in-situ crystallization and layer-by-layer assembly techniques. However, the in-situ approach might not be efficient and economically sustainable when it comes to high demands. Recently, a novel strategy for integrating MOF materials with OF sensing platforms was reported [52], [53]. A UV-curable silicone polymer based on PDMS was employed as the host material for ZIF-8 powder, and the ZIF-8 functionalized polymer was coated on OF sensing platforms, including an etched multimode fiber and a D-shaped single-mode fiber. The optical and mechanical properties of the composite polymer coating were characterized and optimized by adjusting the ZIF- 8/polymer weight ratio. Gas molecules (e.g., CH_4) trapped in the ZIF-8 nanocrystallites modified the RI of the composite polymer coating, resulting in changes in the transmission of the OF sensors. The prototype OF sensors showed an LoD of 1% for detection of CH_4 when N_2 was used as the carrier gas. The proposed coating strategy provided an innovative approach to integrating MOF materials with OF sensing platforms through a fast and cost-effective UV-curing process. The approach should be especially attractive when it comes to distributed chemical sensing where long lengths of OF require the MOF coating.

D. Surface Plasmon Resonance

Evanescent field OF probes constitute portable and miniature counterparts to traditional bulky prism-based microscope systems for the implementation of surface plasmon resonance (SPR) and localized surface plasmon resonance (LSPR) spectroscopy [54]. An SPR-based OF sensor is typically fabricated by coating a thin film of noble metal onto the surface of the OF. The evanescent wave of the OF propagates along the glass-metal interface, and energy transfer from the evanescent wave to the surface plasmon polaritons occurs when their propagation constants match, resulting in the so-called resonance state. Different from SPR, where the lossy waves transmit along a continuous glass-metal interface, LSPR refers to an optical phenomenon caused by light waves trapped within metallic nanostructures (e.g., nanoparticles, NPs). The electrons in the conduction band of the metal oscillate coherently under the illumination of the incident light, resulting in strong localized plasmon oscillations and manifesting as a characteristic extinction spectrum. The resonance frequency of both SPR and LSPR is dependent on the RI of the surrounding medium of the metal layer (continuous films for SPR and NPs for LSPR). Changes in the surrounding RI can be detected by tracking the shifts of the resonance spectrum. Compared to SPR, the distinct advantage of LSPR is the use of NPs that further increases the surface contact area with the surrounding medium, leading to higher sensitivity. SPR and LSPR spectroscopy are widely used for chemical and biological sensing in aqueous environments, and recent progress on plasmonic OF sensors can be found in [54]. However, similar to other OF RI sensors, the utility of plasmonic OF sensors for gas sensing is hindered by two common challenges: 1) the RI differences between different gases or different concentrations of a specific gas are too small to measure; 2) the RI sensors are inherently non-specific, meaning the type of molecules that contribute to the change in the characteristic spectrum cannot be identified. As discussed above, the MOF materials with high porosity and tailorable specificity, which can not only act as a molecule sponge to locally concentrate the gas analyte but also select for a target analyte, are an ideal complement to OF RI sensors including the plasmonic OF sensors for gas sensing.

A plasmonic OF-MOF hydrogen sensor was reported very recently [55]. The sensor was based on a gold-coated silica fiber (thickness, 40 nm; length, 2 cm) decorated by an IRMOF-20 layer, where the former provides the plasmon properties and the latter endows high sensitivity and affinity toward hydrogen molecules. The fabrication and the working principle of the sensor are schematically illustrated in Fig. 13. The key component is that the thickness of the MOF film should be relatively large (~1.2 μm) to generate a sufficient increase in RI surrounding the OF so that the plasmonic resonance of the sensor can be observed in air. The responses of the prototype sensor to various concentrations of hydrogen at room temperature (24°C) were tested. Both the resonance wavelength and intensity in the extinction spectrum exhibited strong and quasilinear dependence on the concentration of hydrogen in the range 0–20% hydrogen/air mixture, as shown in Fig. 14. While above 20%, saturation was observed. In addition to the high sensitivity, the sensor showed very good repeatability over a 2-month period, high response/recovery rate (10/5 s), prominent selectivity to hydrogen in the presence of interference gases such as NO_2 and CO_2, and low-dependence on temperature and humidity. The work employed a simple plasmonic OF configuration for the proof of concept; other configurations such as the tapered fiber, the

D-shaped fiber, and the grating-assisted fiber, are expected to be utilized to further improve the sensitivity [54].

Preliminary work on the development of LSPR-based OF-MOF sensors has also been reported [56]. A cleaved end facet of an optical fiber was first coated with gold NPs (size: ~40 nm) and followed by functionalization with a thin film of HKUST-1. The characteristic spectrum of the prototype sensor showed redshift in response to different concentrations of acetone. Note that although a systematic investigation has yet to be performed for the LSPR-based OF-MOF sensor, the inherent highly localized and intense electromagnetic field of LSPR provides high RI sensitivity that is particularly attractive for chemical sensing. The feasibility of incorporating a MOF thin film in an LSPR device for enhancement of both sensitivity and selectivity was verified using a microscope coverslip-based LSPR sensor [57]. Fig. 15 shows the SEM images of a glass coverslip-based LSPR-MOF sensor. Note that the fabrication of the current LSPR-MOF sensor involved two separate fabrication processes, deposition of NPs and growth of a MOF film on the NPs. An interesting question is whether small metal NPs can be directly incorporated into the MOF for developing LSPR-based sensors, and possibly for generating surface-enhanced Raman scattering effects [58].

E. Other MOF Sensors

In addition to OF devices, other types of optical RI sensing configurations are also explored as platforms for developing MOF sensors. For example, a CO_2 sensor was developed based on a bimodal optical waveguide coated with ZIF-8 NPs [59]. A hybrid photonic band-gap (PBG) structure fabricated by stacking alternating layers of MOF and indium tin oxide was reported, achieving high optical reflectivities of 80% [60]. Both PBG wavelength and the reflection intensity exhibited observable changes upon exposure to specific solvents, making the porous Bragg stacks a potential chemical sensor device. Another interesting strategy integrated a colloidal crystal (CC) as the signal transducer and a MOF as the sensing material [61], [62]. CCs are capable of reflecting the incident light at a specific wavelength (i.e., the stop band) due to the periodic modulation of the RI in the arrayed crystals, and the stop band wavelength is dependent on the effective RI of the crystals. Coating the crystals with a MOF endows the CC with sorption capabilities that can be used for selective sensing. Growing CC thin films on the endface of an OF and then depositing a thin film of MOF on the CC could be another pathway to develop miniature and remote OF-MOF chemical sensor probes.

Apart from optical spectroscopy, microwave dielectric spectroscopy constitutes another technique that is widely used to characterize the EM properties of materials at microwave frequencies (e.g., GHz). Compared to OF sensors, microwave resonators have some interesting features that are advantageous for sensing, such as low system cost, robustness, ease of fabrication, and wireless connectivity. Microwave resonator-based MOF devices were reported as gas sensors [63]–[65], where the MOFs, typically in the form of thin beds, were used as the sensitive materials. Note that constructing such a microwave resonator MOF device is easier than engineering an OF-MOF device, since a thin bed of MOF can be simply physically attached to the microwave resonator. Additionally, non-contact

measurements of dielectric properties of MOFs in response to different concentrations of gas analytes could also be achieved by microwave resonators [65]. However, the response rate of microwave MOF sensors is typically lower than that of thin film-based OF-MOF sensors, since the size dimensions of the sensitive layer increases drastically from thin films (1 μm scale) to thin beds (hundreds of μm).

III. Conclusion and Perspective

This paper reviewed recent progress on MOFs as chemosensory materials for the development of OF chemical sensors. Thanks to the recent advancement of MOF thin-film growth techniques, e.g., in-situ crystallization and layer-by-layer assembly methods, thin films of MOFs with controlled thickness and surface morphology can be directly coated onto the surfaces of OFs, laying the groundwork for OF-MOF sensors. The fundamental principle of OF-MOF sensors relies on the dependence of the effective RI of the MOF on the amount and RI of guest molecules contained in the inherent porosity of MOF. Changes in the RI of a MOF are detected by various optical methods, as categorized in this review, including interferometry, evanescent field sensing (e.g., LPGs-based), transmission spectroscopy, SPR, and LSPR. The MOFs in these sensor devices serve two functions: 1) they act as molecular sponges that increase the local concentration of the analyte due to extensive adsorption porosity; 2) they endow the sensor with the ability to selectively respond to a target analyte due to tailorable pore sizes and chemical properties. Particularly, in the FPI sensing configuration, the MOF layer also functions as the FP cavity that produces the characteristic spectrum of the sensor. Currently, the limiting aspect of OF-MOF sensors is the high system cost of an optical fiber sensing system (e.g., the interrogator) in comparison to an electronic sensor system. Also, the size of an electronic sensor system is much more compact than an optical fiber sensor system. However, compared to electronic sensors, the OF-MOF sensors do have some unique features, such as their high sensitivity, small probe head size, remote sensing capability, and no requirements on the conductivity parameter of the selected MOF [1], [7].

Another advantage of OF sensors, compared to electronic sensors, is their capability for multiplexing and distributed sensing, which has not yet been explored for OF-MOF sensors. Despite exceptional tunability of pore size/shape and chemical properties of MOFs, the goal of highly selective recognition of a single target guest remains challenging and continues to prove difficult, if not impossible. Intrigued by the electronic- (E-) nose technologies, a sensor array composed of different MOF materials might be an attractive solution to address the circumstances of multi-component adsorbate compositions in most MOF materials [66]–[69]. The key strategy for designing a MOF array sensor is to utilize highly diverse MOFs with distinct affinities for target molecules, where each of the MOF materials interacts with the analyte mixture differently to produce a unique overall fingerprint. Advanced analytical techniques entailing pattern recognition and classification approaches (e.g., machine learning) can be used to analyze the sensor array’s convoluted response by mapping a unique fingerprint to each composition of individual analytes in a multi-component mixture. Importantly, the multiplexing capability of OF sensors provides a unique opportunity and convenient pathway to develop such an OF-MOF sensor array [70], [71]. For example, the recently developed optical carrier based microwave reflectometry

technique can be an ideal candidate [72], where tens of high-resolution RI probes (with a resolution of 3.6 ppm in the refractive index unit) can be multiplexed. Essentially, the OF-MOF sensor array may revolutionize the field of the E-nose because of the improved sensitivity and especially the selectivity afforded by the MOF materials. On the other hand, the OF-MOF sensor array employing one MOF type could be applicable for multipoint leak monitoring along natural gas pipelines due to its multiplexing and remote sensing capabilities.

Previous work showed that the diffusion of guest molecules into MOF host pores is highly anisotropic [31], [73], and the orientations of different molecules adsorbed within the micropores are different. The orientations of molecules interacting with MOF or zeolite adsorption sites can be implicated for sensing specific adsorbates. The motif of coupling a MOF or zeolite single crystal to an optical fiber provides access to molecular-level details of guest-host interactions because it combines the geometrical uniformity of the orientations and positions of each adsorption site inherent to a single crystal and the unique capabilities of miniaturized polarized light probing techniques. OF-based polarized-light spectroscopy can provide insights into single- and multi-component adsorption processes in real-time. It will also be feasible to identify each guest molecule in a mixture of multiple guests by analyzing the changes in the polarization of the polarized light beam. The uniqueness of the nine-element tensor that describes the permittivity features of a MOF or zeolite micro-crystal host with adsorbed guests makes it possible to study the weighted-average dynamic occupancies and orientations of guest molecules in the micropores of the MOF or zeolite host, which in turn affords the possibility to identify individual molecules within a MOF or zeolite cage containing multi-component mixtures of guest molecules [74]–[79]. On the other hand, the polarization of the light beam output from an OF-single crystal MOF or zeolite structure will vary with the type and amount of adsorbed guest molecules, revealing a unique strategy to develop tunable fiber-optic in-line polarizer microdevices based on single-crystal MOF or zeolite materials.

The research field of OF-MOF chemical sensors is still at a very early and exploratory stage. Several ultra-sensitive OF RI sensing platforms have not been explored for MOF sensors, such as microfibers and tilted fiber Bragg gratings. Particularly, microfibers with a diameter close to or below the wavelength of the transmitting light exhibit unique properties that are advantageous for sensing, such as ultracompactness, tailorable optical confinement and dispersion, and greatly enhanced evanescent fields [80]. Operating a microfiber-based interferometer at the dispersion turning point was demonstrated with an ultrahigh RI sensitivity of up to 95,836 nm/RI unit [81], making it an excellent candidate for OF-MOF chemical sensors. Another promising direction is to combine MOFs with miniature and portable OF-based Raman spectroscopy. Raman spectroscopy, known as vibrational spectroscopy that can provide a molecular fingerprint, is a powerful chemical and biological sensing modality with high sensitivity and specificity for molecular identifications of liquids, solids, and gases [82]. The integration of Raman spectroscopy with fiber optics combines the unique strengths of each and enables easy deployment in remote and environmentally harsh sites for in-situ chemical detection. Coupling MOFs with OF Raman systems will not only improve the sensitivity and LoD of existing Raman systems owing to the pre-concentrations achieved by MOFs, but also potentially could enhance the

chemical selectivity due to the fusion of a two-fold specificity, one from Raman vibrational spectroscopy and the other from MOF molecular exclusion capabilities. The possibility of MOFs serving as novel substrates for surface-enhanced Raman scattering (SERS) can further increase the performance of OF-MOF Raman systems [58], [83], [84]. An exemplary implementation of the OF-MOF Raman sensor could be the direct deposition of MOF thin films along a specially designed OF platform that is highly evanescent for a certain length. A MOF coating would essentially function as the OF's cladding, which can partition and concentrate the target analyte within the electrical field of the propagating EM wave. The Raman scattering of the analyte generated in the cladding (i.e., the MOF coating) due to the enhanced wave-matter interaction accumulates along the length of the MOF film, enabling molecular-specific detection of parts-per-billion analyte concentrations [85].

Although the recent proliferation of MOF thin-film growth techniques has fundamentally increased the momentum of MOF sensors, the major challenge for developing MOF sensors including OF-MOF sensors is the integration of MOFs into sensing substrates comprising a two- or three-dimensional architecture. Currently, the widely used approach for coating MOF materials onto an OF involves in-situ crystallization and layer-by-layer assembly techniques. The in-situ growth method is convenient, but it is not efficient and it is also time-consuming, especially when long-lengths (>10 cm) and thick films (>10 μm) are required. Additionally, the bonding strength between a MOF film and an OF surface and the thermal and mechanical properties of the MOF films have not been systematically investigated, which are crucial for the performance of OF-MOF sensors. The recently developed polymer matrix-assisted coating method might be an alternative approach with its own advantages [52]. It is envisioned that with the advancement of this aspect of MOF science, i.e., MOF thin-film coating methods, the field of OF-MOF sensors will pick up momentum and see steady growth in the coming years.

Acknowledgments

Research reported in this publication was supported by the National Institutes of Health under award number 1U01HL152410–01.

Biography

ChenZhu (Member, IEEE) received the B.E. degree in optoelectronics information engineering from Huazhong University of Science and Technology, Wuhan, China, in 2015, and the Ph.D. degree in electrical engineering from Missouri University of Science and Technology, Missouri, USA, in 2021. He is an Assistant Research Professor with the Department of Electrical and Computer Engineering, Missouri University of Science and Technology. His research interest is focused on the development of photonic and microwave devices for sensing applications in harsh environments. He was a recipient of the IEEE Instrumentation and Measurement Society Graduate Fellowship Award from 2018 to 2019 and the 2020 IEEE St. Louis Section Outstanding Graduate Student Award.

Rex E. Gerald II received the B.A. degree in chemistry from the University of Chicago (UC), Chicago, IL, USA, and the conjoint Ph.D. degree in physical chemistry from the University of Illinois at Chicago (UIC) and the Max Planck Institute (MPI), Heidelberg.

He is a Research Professor with the Lightwave Technology Laboratory, Department of Electrical and Computer Engineering, Missouri University of Science and Technology (MS&T). He holds 26 U.S. patents and coauthored more than 50 publications from research investigations conducted at UC, UIC, MPI, Argonne National Laboratory, and Missouri S&T.

Jie Huang (Senior Member, IEEE) is the Director of the Lightwave Technology Laboratory and an Assistant Professor of Electrical and Computer Engineering with the Missouri University of Science and Technology. He has performed research in instrumentation and measurement for more than ten years. He authored or coauthored over 80 refereed articles, 60 conference papers, one book chapter, and ten U.S. patent applications (five are issued) all in the area of advanced sensors. His research interests include development of optical and microwave sensors and instrumentation for applications in energy, intelligent infrastructures, clean-environment, and biomedical sensing.

References

[1]. Kreno LE, Leong K, Farha OK, Allendorf M, Van Duyne RP, and Hupp JT, “Metal–organic framework materials as chemical sensors,” Chem. Rev, vol. 112, no. 2, pp. 1105–1125, 2012. [PubMed: 22070233]

[2]. Lee J, Farha OK, Roberts J, Scheidt KA, Nguyen ST, and Hupp JT, “Metal–organic framework materials as catalysts,” Chem. Soc. Rev, vol. 38, no. 5, pp. 1450–1459, 2009. [PubMed: 19384447]

[3]. Zhu Q-L and Xu Q, “Metal–organic framework composites,” Chem. Soc. Rev, vol. 43, no. 16, pp. 5468–5512, 2014. [PubMed: 24638055]

[4]. Zhou H-C, Long JR, and Yaghi OM, “Introduction to metal–organic frameworks,” ed: ACS Publications, 2012.

[5]. Kang Z, Fan L, and Sun D, “Recent advances and challenges of metal–organic framework membranes for gas separation,” Journal of Materials Chemistry A, vol. 5, no. 21, pp. 10073–10091, 2017.

[6]. Suh MP, Park HJ, Prasad TK, and Lim D-W, “Hydrogen storage in metal–organic frameworks,” Chem. Rev, vol. 112, no. 2, pp. 782–835, 2012. [PubMed: 22191516]

[7]. Chidambaram A and Stylianou KC, “Electronic metal–organic framework sensors,” Inorganic Chemistry Frontiers, vol. 5, no. 5, pp. 979–998, 2018.

[8]. Hu Z, Deibert BJ, and Li J, “Luminescent metal–organic frameworks for chemical sensing and explosive detection,” Chem. Soc. Rev, vol. 43, no. 16, pp. 5815–5840, 2014. [PubMed: 24577142]

[9]. Zhang L-T, Zhou Y, and Han S-T, “The role of metal–organic framework in electronic sensors,” Angewandte Chemie, 2020.

[10]. Bender F, Barié N, Romoudis G, Voigt A, and Rapp M, “Development of a preconcentration unit for a SAW sensor micro array and its use for indoor air quality monitoring,” Sensors and Actuators B : Chemical, vol. 93, no. 1–3, pp. 135–141, 2003.

[11]. Lee H et al. , “A Chromo-Fluorogenic Tetrazole-Based CoBr2 Coordination Polymer Gel as a Highly Sensitive and Selective Chemosensor for Volatile Gases Containing Chloride,” Chemistry–A European Journal, vol. 17, no. 10, pp. 2823–2827, 2011. [PubMed: 21312303]

[12]. Goeders KM, Colton JS, and Bottomley LA, “Microcantilevers: sensing chemical interactions via mechanical motion,” Chem. Rev, vol. 108, no. 2, pp. 522–542, 2008. [PubMed: 18229951]

[13]. Khoshaman AH and Bahreyni B, “Application of metal organic framework crystals for sensing of volatile organic gases,” Sensors and Actuators B : Chemical, vol. 162, no. 1, pp. 114–119, 2012.

[14]. Allendorf MD et al. , “Stress-induced chemical detection using flexible metal- organic frameworks,” J. Am. Chem. Soc, vol. 130, no. 44, pp. 14404–14405, 2008. [PubMed: 18841964]

[15]. Achmann S, Hagen G, Kita J, Malkowsky IM, Kiener C, and Moos R, "Metal-organic frameworks for sensing applications in the gas phase," Sensors, vol. 9, no. 3, pp. 1574–1589, 2009. [PubMed: 22573973]

[16]. Kim K-J, Lu P, Culp JT, and Ohodnicki PR, "Metal–organic framework thin film coated optical fiber sensors: a novel waveguide-based chemical sensing platform," ACS sensors, vol. 3, no. 2, pp. 386–394, 2018. [PubMed: 29303556]

[17]. Zhao Y, Li X.-g., Zhou X, and Zhang Y.-n., "Review on the graphene based optical fiber chemical and biological sensors," Sensors and Actuators B : Chemical, vol. 231, pp. 324–340, 2016.

[18]. Joe H-E, Yun H, Jo S-H, Jun MB, and Min B-K, "A review on optical fiber sensors for environmental monitoring," International journal of precision engineering and manufacturing-green technology, vol. 5, no. 1, pp. 173–191, 2018.

[19]. Lee B, "Review of the present status of optical fiber sensors," Optical fiber technology, vol. 9, no. 2, pp. 57–79, 2003.

[20]. Zhu C, Gerald RE, and Huang J, "Progress Towards Sapphire Optical Fiber Sensors for High-temperature Applications," IEEE Trans. Instrum. Meas, 2020.

[21]. Xia T et al. , "A fluorometric metal-organic framework oxygen sensor: from sensitive powder to portable optical fiber device," Microporous and Mesoporous Materials, vol. 305, p. 110396, 2020.

[22]. Ohira S-I et al. , "A fiber optic sensor with a metal organic framework as a sensing material for trace levels of water in industrial gases," Anal. Chim. Acta, vol. 886, pp. 188–193, 2015. [PubMed: 26320652]

[23]. Zhao L et al. , "A luminescent metal–organic framework integrated hydrogel optical fibre as a photoluminescence sensing platform for fluorescence detection," Journal of Materials Chemistry C, vol. 7, no. 4, pp. 897–904, 2019.

[24]. Lee BH et al. , "Interferometric fiber optic sensors," sensors, vol. 12, no. 3, pp. 2467–2486, 2012. [PubMed: 22736961]

[25]. Lu G and Hupp JT, "Metal- organic frameworks as sensors: a ZIF-8 based Fabry- Pérot device as a selective sensor for chemical vapors and gases," J. Am. Chem. Soc, vol. 132, no. 23, pp. 7832–7833, 2010. [PubMed: 20486704]

[26]. Nazari M et al. , "UiO-66 MOF end-face-coated optical fiber in aqueous contaminant detection," Opt. Lett, vol. 41, no. 8, pp. 1696–1699, 2016. [PubMed: 27082322]

[27]. Nazari M, Amini A, Hill MR, Cheng C, and Samali B, "Physical and chemical reaction sensing in a mixed aqueous solution via metal-organic framework thin-film coated optical fiber," Microwave and Optical Technology Letters, vol. 62, no. 1, pp. 72–77, 2020.

[28]. Kim H-T, Hwang W, Liu Y, and Yu M, "Ultracompact gas sensor with metal-organic-framework-based differential fiber-optic Fabry-Perot nanocavities," Opt. Express, vol. 28, no. 20, pp. 29937–29947, 2020. [PubMed: 33114882]

[29]. Wang H et al. , "Gas Sensing Materials Roadmap," Journal of Physics: Condensed Matter, 2021.

[30]. Zhu C, Perman JA, Gerald RE, Ma S, and Huang J, "Chemical Detection Using a Metal–Organic Framework Single Crystal Coupled to an Optical Fiber," ACS applied materials & interfaces, vol. 11, no. 4, pp. 4393–4398, 2019. [PubMed: 30600993]

[31]. Lee CY et al. , "Kinetic separation of propene and propane in metal-organic frameworks: Controlling diffusion rates in plate-shaped crystals via tuning of pore apertures and crystallite aspect ratios," J. Am. Chem. Soc, vol. 133, no. 14, pp. 5228–5231, 2011. [PubMed: 21417272]

[32]. Sun Z et al. , "Thermal stability of optical fiber metal organic framework based on graphene oxide and nickel and its hydrogen adsorption application," Opt. Express, vol. 26, no. 24, pp. 31648–31656, 2018. [PubMed: 30650748]

[33]. Zhu G et al. , "A metal-organic zeolitic framework with immobilized urease for use in a tapered optical fiber urea biosensor," Microchimica Acta, vol. 187, no. 1, p. 72, 2020.

[34]. Chiavaioli F et al. , "Sol–gel-based titania–silica thin film overlay for long period fiber grating-based biosensors," Anal. Chem, vol. 87, no. 24, pp. 12024–12031, 2015. [PubMed: 26548589]

[35]. Shu X, Zhang L, and Bennion I, "Sensitivity characteristics of long-period fiber gratings," Journal of Lightwave Technology, vol. 20, no. 2, pp. 255–266, 2002.

[36]. Esposito F, Srivastava A, Sansone L, Giordano M, Campopiano S, and Iadicicco A, “Label-free biosensors based on long period fiber gratings: a review,” IEEE Sens. J, 2020.

[37]. Zhao X-W and Wang Q, “Mini review: Recent advances in long period fiber grating biological and chemical sensors,” Instrumentation Science & Technology, vol. 47, no. 2, pp. 140–169, 2019.

[38]. Hromadka J, Tokay B, James S, Tatam RP, and Korposh S, “Optical fibre long period grating gas sensor modified with metal organic framework thin films,” Sensors and Actuators B : Chemical, vol. 221, pp. 891–899, 2015.

[39]. Hromadka J, Tokay B, Correia R, Morgan SP, and Korposh S, “Highly sensitive volatile organic compounds vapour measurements using a long period grating optical fibre sensor coated with metal organic framework ZIF-8,” Sensors and Actuators B : Chemical, vol. 260, pp. 685–692, 2018.

[40]. Hromadka J, Tokay B, Correia R, Morgan SP, and Korposh S, “Highly sensitive ethanol vapour measurements using a fibre optic sensor coated with metal organic framework ZIF-8,” in 2017 IEEE SENSORS, 2017: IEEE, pp. 1–3.

[41]. Acha ND et al. , “Detection of Ethanol in Human Breath Using Optical Fiber Long Period Grating Coated with Metal-Organic Frameworks,” in Multidisciplinary Digital Publishing Institute Proceedings, 2017, vol. 1, no. 4, p. 474.

[42]. Hromadka J, Tokay B, James S, and Korposh S, “Metal-organic framework thin films on a surface of optical fibre long period grating for chemical sensing,” in 2017 25th Optical Fiber Sensors Conference (OFS), 2017: IEEE, pp. 1–4.

[43]. Hromadka J, Tokay B, Correia R, Morgan SP, and Korposh S, “Carbon dioxide measurements using long period grating optical fibre sensor coated with metal organic framework HKUST-1,” Sensors and Actuators B : Chemical, vol. 255, pp. 2483–2494, 2018.

[44]. Zhu G, Zhang M, Lu L, Lou X, Dong M, and Zhu L, “Metal-organic framework/enzyme coated optical fibers as waveguide-based biosensors,” Sensors and Actuators B : Chemical, vol. 288, pp. 12–19, 2019.

[45]. Wu J et al. , “Nanoscale light–matter interactions in metal–organic frameworks cladding optical fibers,” Nanoscale, vol. 12, no. 18, pp. 9991–10000, 2020. [PubMed: 32134070]

[46]. Bürck J, Conzen J-P, and Ache H-J, “A fiber optic evanescent field absorption sensor for monitoring organic contaminants in water,” Fresenius J. Anal. Chem, vol. 342, no. 4–5, pp. 394–400, 1992.

[47]. Lan X et al. , “Fiber ring laser interrogated zeolite-coated singlemode-multimode-singlemode structure for trace chemical detection,” Opt. Lett, vol. 37, no. 11, pp. 1998–2000, 2012. [PubMed: 22660100]

[48]. Kim K-J et al. , “Alkylamine-Integrated Metal–Organic Framework-Based Waveguide Sensors for Efficient Detection of Carbon Dioxide from Humid Gas Streams,” ACS applied materials & interfaces, vol. 11, no. 36, pp. 33489–33496, 2019. [PubMed: 31429267]

[49]. Chong X et al. , “Ultra-Sensitive CO2 Fiber-Optic Sensors Enhanced by Metal-Organic Framework Film,” in CLEO: QELS_Fundamental Science, 2016: Optical Society of America, p. JTu5A. 138.

[50]. Chong X, Kim K-J, Ohodnicki PR, Li E, Chang C-H, and Wang AX, “Ultrashort near-infrared fiber-optic sensors for carbon dioxide detection,” IEEE Sens. J, vol. 15, no. 9, pp. 5327–5332, 2015.

[51]. Chong X et al. , “Near-infrared absorption gas sensing with metal-organic framework on optical fibers,” Sensors and Actuators B : Chemical, vol. 232, pp. 43–51, 2016.

[52]. Cao R et al. , “Metal-organic framework functionalized polymer coating for fiber optical methane sensors,” Sensors and Actuators B : Chemical, vol. 324, p. 128627, 2020.

[53]. Cao R et al., “Fiber Optical Sensor for Methane Detection Based on Metal-Organic Framework/ Silicone Polymer Coating,” in CLEO: Applications and Technology, 2018: Optical Society of America, p. JW2A. 168.

[54]. Caucheteur C, Guo T, and Albert J, “Review of plasmonic fiber optic biochemical sensors: improving the limit of detection,” Anal. Bioanal. Chem, vol. 407, no. 14, pp. 3883–3897, 2015. [PubMed: 25616701]

[55]. Miliutina E et al. , “Fast and All-Optical Hydrogen Sensor Based on Gold-Coated Optical Fiber Functionalized with Metal–Organic Framework Layer,” ACS sensors, vol. 4, no. 12, pp. 3133–3140, 2019. [PubMed: 31793768]

[56]. Liu L, He C, Morgan SP, Correia R, and Korposh S, “A fiber-optic localized surface plasmon resonance (LSPR) sensor anchored with metal organic framework (HKUST-1) film for acetone sensing,” in Seventh European Workshop on Optical Fibre Sensors, 2019, vol. 11199: International Society for Optics and Photonics, p. 111990Z.

[57]. Kreno LE, Hupp JT, and Van Duyne RP, “Metal- organic framework thin film for enhanced localized surface plasmon resonance gas sensing,” Anal. Chem, vol. 82, no. 19, pp. 8042–8046, 2010. [PubMed: 20839787]

[58]. Sugikawa K, Furukawa Y, and Sada K, “SERS-active metal–organic frameworks embedding gold nanorods,” Chem. Mater, vol. 23, no. 13, pp. 3132–3134, 2011.

[59]. Chocarro-Ruiz B et al. , “A CO 2 optical sensor based on self-assembled metal–organic framework nanoparticles,” Journal of Materials Chemistry A, vol. 6, no. 27, pp. 13171–13177, 2018.

[60]. Liu J et al. , “Monolithic high performance surface anchored metal-organic framework Bragg reflector for optical sensing,” Chem. Mater, vol. 27, no. 6, pp. 1991–1996, 2015.

[61]. Lu G et al. , “Fabrication of Metal-Organic Framework-Containing Silica-Colloidal Crystals for Vapor Sensing,” Advanced Materials, vol. 23, no. 38, pp. 4449–4452, 2011. [PubMed: 21858878]

[62]. Li L, Jiao X, Chen D, Lotsch BV, and Li C, “Facile Fabrication of Ultrathin Metal–Organic Framework-Coated Monolayer Colloidal Crystals for Highly Efficient Vapor Sensing,” Chem. Mater, vol. 27, no. 22, pp. 7601–7609, 2015.

[63]. Zarifi MH, Gholidoust A, Abdolrazzaghi M, Shariaty P, Hashisho Z, and Daneshmand M, “Sensitivity enhancement in planar microwave active-resonator using metal organic framework for CO2 detection,” Sensors and Actuators B : Chemical, vol. 255, pp. 1561–1568, 2018.

[64]. Zhu C, Gerald II RE, Chen Y, and Huang J, “Metal-organic framework portable chemical sensor,” Sensors and Actuators B : Chemical, vol. 321, p. 128608, 2020.

[65]. Zarifi MH, Shariaty P, Hashisho Z, and Daneshmand M, “A non-contact microwave sensor for monitoring the interaction of zeolite 13X with CO2 and CH4 in gaseous streams,” Sensors and Actuators B : Chemical, vol. 238, pp. 1240–1247, 2017.

[66]. Sousa R and Simon CM, “Evaluating the fitness of combinations of adsorbents for quantitative gas sensor arrays,” ACS sensors, 2020.

[67]. Feng S et al. , “Review on smart gas sensing technology,” Sensors, vol. 19, no. 17, p. 3760, 2019.

[68]. Gustafson JA and Wilmer CE, “Intelligent selection of metal–organic framework arrays for methane sensing via genetic algorithms,” ACS sensors, vol. 4, no. 6, pp. 1586–1593, 2019. [PubMed: 31124354]

[69]. Röck F, Barsan N, and Weimar U, “Electronic nose: current status and future trends,” Chem. Rev, vol. 108, no. 2, pp. 705–725, 2008. [PubMed: 18205411]

[70]. Du Y, Jothibasu S, Zhuang Y, Zhu C, and Huang J, “Rayleigh backscattering based macrobending single mode fiber for distributed refractive index sensing,” Sensors and Actuators B : Chemical, vol. 248, pp. 346–350, 2017.

[71]. Ding Z et al. , “Distributed refractive index sensing based on tapered fibers in optical frequency domain reflectometry,” Opt. Express, vol. 26, no. 10, pp. 13042–13054, 2018. [PubMed: 29801337]

[72]. He X, Ran Z, Yang T, Xiao Y, Wang Y, and Rao Y, “Temperature-insensitive fiber-optic tip sensors array based on OCMR for multipoint refractive index measurement,” Opt. Express, vol. 27, no. 7, pp. 96659675, 2019.

[73]. Greenaway A et al. , “In situ Synchrotron IR Microspectroscopy of CO2 Adsorption on Single Crystals of the Functionalized MOF Sc2 (BDC-NH2) 3,” Angewandte Chemie International Edition, vol. 53, no. 49, pp. 13483–13487, 2014. [PubMed: 25382542]

[74]. Jameson CJ, Jameson AK, Gerald R, and de Dios AC, “Nuclear magnetic resonance studies of xenon clusters in zeolite NaA,” The J. Chem. Phys, vol. 96, no. 3, p. 1676, 1992.

[75]. Jameson CJ, Jameson AK, Gerald RE, and Lim H-M, “Anisotropic Xe chemical shifts in zeolites. The role of intra-and intercrystallite diffusion,” The Journal of Physical Chemistry B, vol. 101, no. 42, pp. 8418–8437, 1997.

[76]. Jameson AK, Jameson CJ, and Gerald RE, “Cage-to-cage migration rates of Xe atoms in zeolite NaA from magnetization transfer experiments and simulations,” The J. Chem. Phys, vol. 101, no. 3, pp. 1775–1786, 1994.

[77]. Jameson AK, Jameson CJ, de Dios AC, Oldfield E, Gerald II RE, and Turner GL, “129Xe Magic-angle spinning spectra of xenon in zeolite NaA direct observation of mixed clusters of co-adsorbed species,” Solid State Nucl. Magn. Reson, vol. 4, no. 1, pp. 1–12, 1995. [PubMed: 7894978]

[78]. Jameson CJ, Jameson AK, de Dios AC, Gerald RE, Lim H-M, and Kostikin P, “Application of Nuclear Shielding Surfaces to the Fundamental Understanding of Adsorption and Diffusion in Microporous Solids,” ACS Publications, 1999.

[79]. Gerald RE, “Solid-State Nuclear Magnetic Resonance,” Encyclopedia of Analytical Chemistry: Applications, Theory and Instrumentation, pp. 1–36, 2006.

[80]. Lou J, Wang Y, and Tong L, “Microfiber optical sensors: A review,” Sensors, vol. 14, no. 4, pp. 5823–5844, 2014. [PubMed: 24670720]

[81]. Sun L-P et al. , “Ultra-high sensitivity of dual dispersion turning point taper-based Mach-Zehnder interferometer,” Opt. Express, vol. 27, no. 16, pp. 23103–23111, 2019. [PubMed: 31510592]

[82]. McNay G, Eustace D, Smith WE, Faulds K, and Graham D, “Surface-enhanced Raman scattering (SERS) and surface-enhanced resonance Raman scattering (SERRS): a review of applications,” Applied spectroscopy, vol. 65, no. 8, pp. 825–837, 2011. [PubMed: 21819771]

[83]. Yu TH, Ho CH, Wu CY, Chien CH, Lin CH, and Lee S, “Metal–organic frameworks: a novel SERS substrate,” J. Raman Spectrosc, vol. 44, no. 11, pp. 1506–1511, 2013.

[84]. Meilikhov M, Yusenko K, Esken D, Turner S, Van Tendeloo G, and Fischer RA, “Metals@ MOFs–loading MOFs with metal nanoparticles for hybrid functions,” Eur. J. Inorg. Chem, vol. 2010, no. 24, pp. 3701–3714, 2010.

[85]. Holmstrom SA et al. , “Trace gas Raman spectroscopy using functionalized waveguides,” Optica, vol. 3, no. 8, pp. 891–896, 2016.

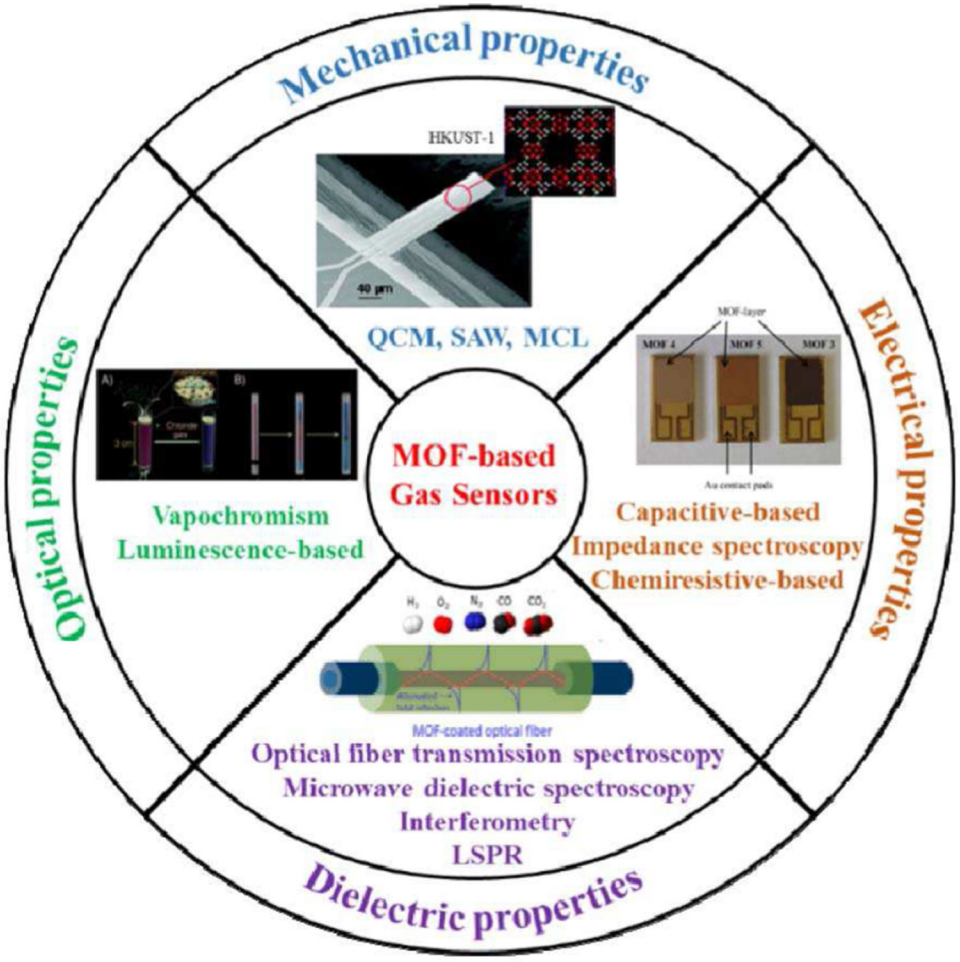

Fig. 1.

Schematic illustration summarizing current MOF-based chemical sensor types based on four different sensing principles. QCM, quartz crystal microbalance; SAW, surface acoustic wave; MCL, microcantilever; LSPR, localized surface plasmon resonances. The figure in the top quadrant shows a microcantilever coated with an HKUST-1 film used for detecting EtOH and CO_2. Reprinted with permission from [14]. Copyright (2008) American Chemical Society. The figure in the right quadrant shows MOF films deposited on interdigitated electrodes for sensing hydrophilic gases. Reprinted with permission from [15]. Copyright (2009) MDPI AG. The figure in the bottom quadrant shows a MOF film coated on a reduced-diameter optical fiber for detecting CO_2. Reprinted with permission from [16]. Copyright (2018) American Chemical Society. The figure in the left quadrant illustrates the color evolution of a MOF-coated capillary tube when it is exposed to 100 mM of chlorine gas. Reprinted with permission from [11]. Copyright (2011) John Wiley and Sons.

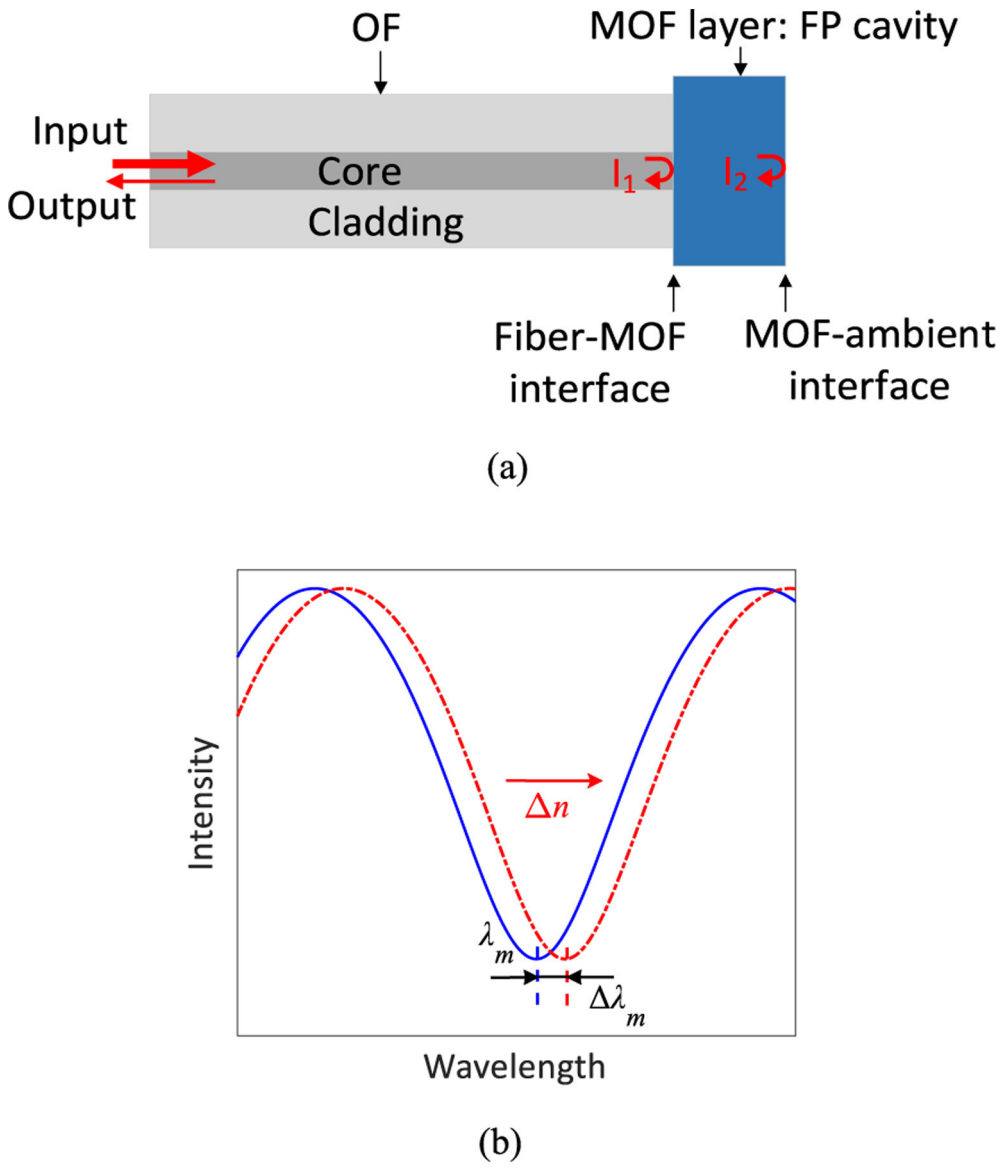

Fig. 2.

Illustration of the FPI-based OF-MOF chemical sensor and sensor output. (a) Schematic of the sensor configuration. (b) Illustration of the sensor output before (blue) and after (red) adsorption of guest molecules by the MOF layer.

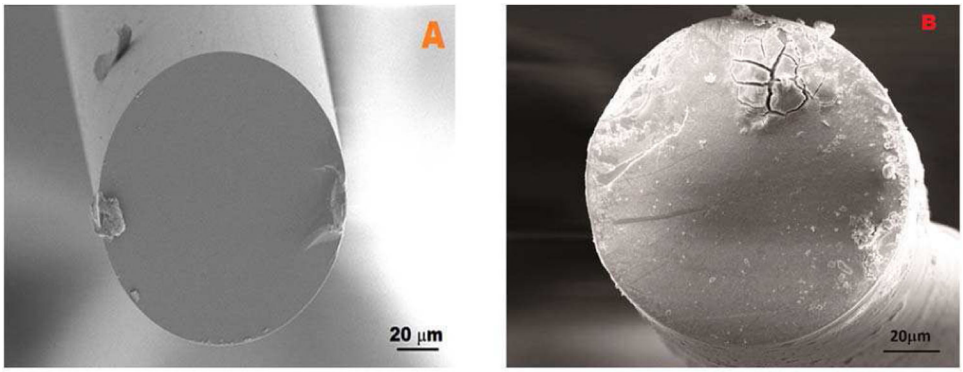

Fig. 3.

SEM images of UiO-66 coated OF. Reprinted with permission from [26] © The Optical Society. (a) Bare fiber. (b) OF with UiO-66 film deposited on the endface.

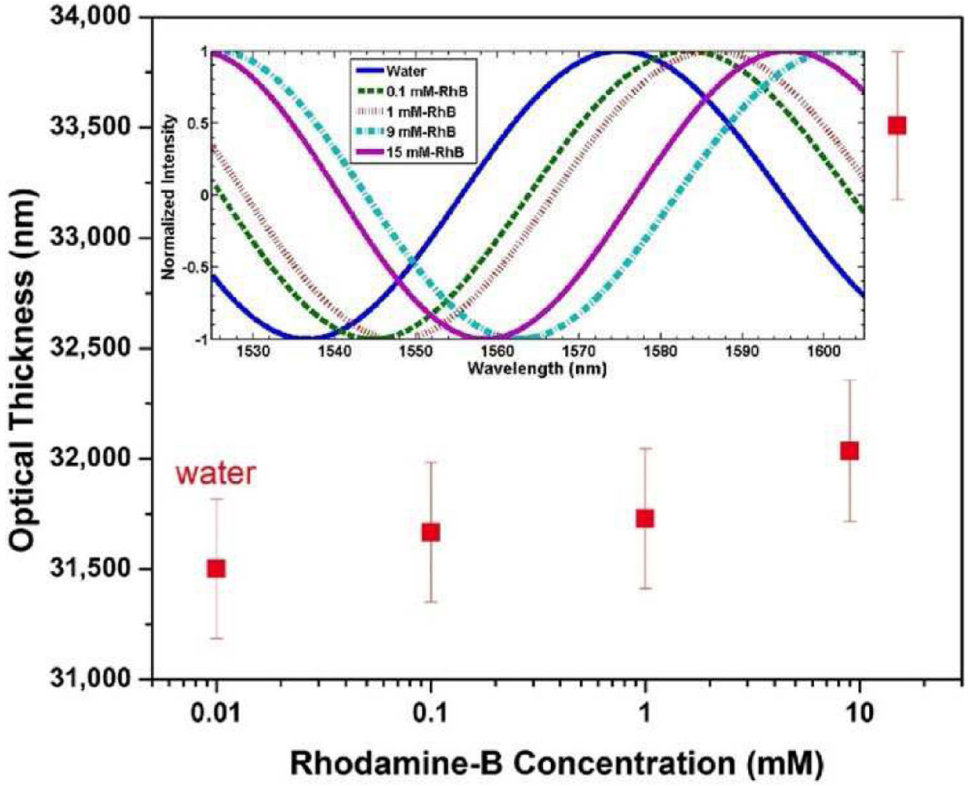

Fig. 4.

Responses of the UiO-66 MOF-coated OF tip sensor to various concentrations of RhB in DI water. Reprinted with permission from [26] © The Optical Society. The inset shows the measured interferograms of the device for different concentrations of RhB.

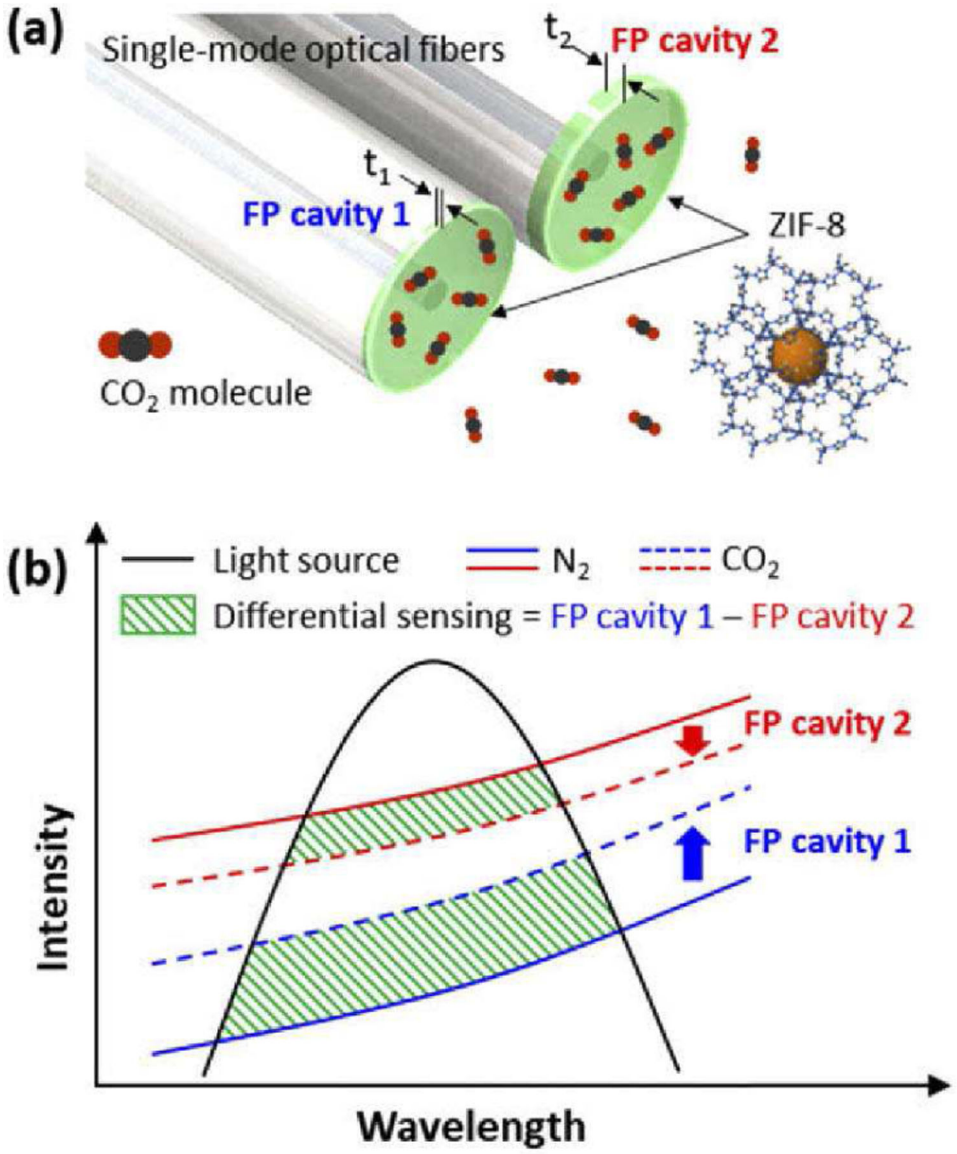

Fig. 5.

Schematic drawing of a differential FP nanocavities-based OF-MOF sensor and graph illustrating the scheme for the principle of operation. Reprinted with permission from [28] © The Optical Society. (a) Schematic of the sensor device. (b) Illustration of the differential interrogation scheme. The reflection intensity of FP cavity 1/cavity 2 increases/decreases as the ambient gas changes from N_2 to CO_2. The sensitivity can be enhanced by measuring the intensity difference between the two cavities. The solid black curve depicts the spectral profile of a broadband light source.

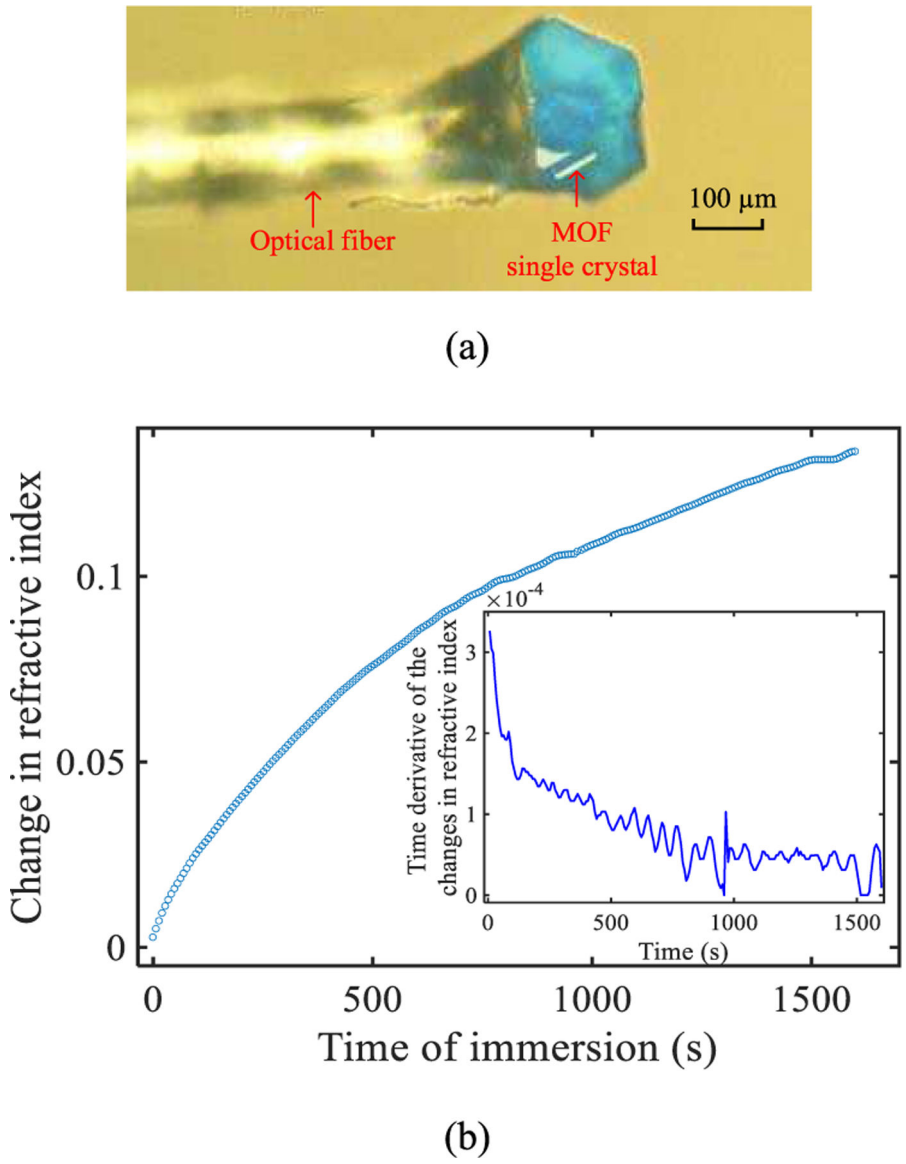

Fig. 6.

A MOF single crystal-based OF-MOF FPI sensor. Reprinted with permission from [30]. Copyright (2019) American Chemical Society. (a) Photograph of a prototype MOF single crystal-based OF-MOF sensor. (b) Change in RI vs. time caused by the adsorption of pure nitrobenzene by a single crystal of HKUST-1 MOF attached to the enface of an OF.

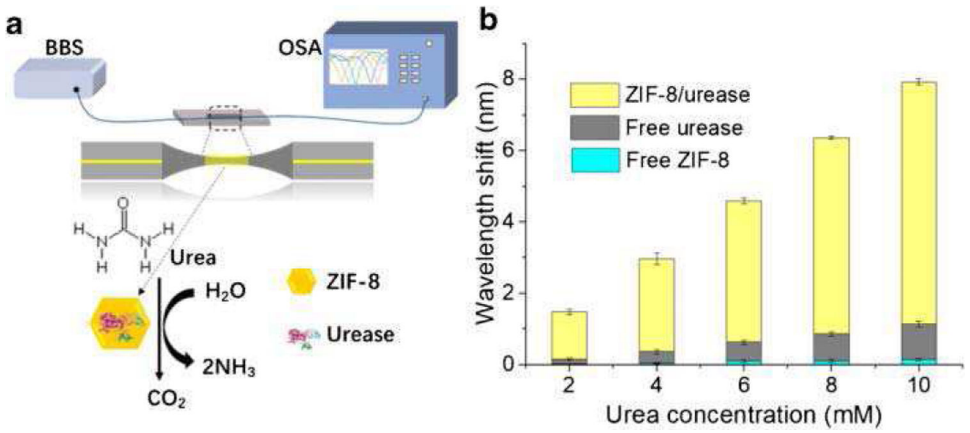

Fig. 7.

SNS-based OF-MOF biosensor [33]. (a) Schematic of the experimental setup and the mechanism for urea detection. (b) Wavelength shift with respect to different concentrations of urea.

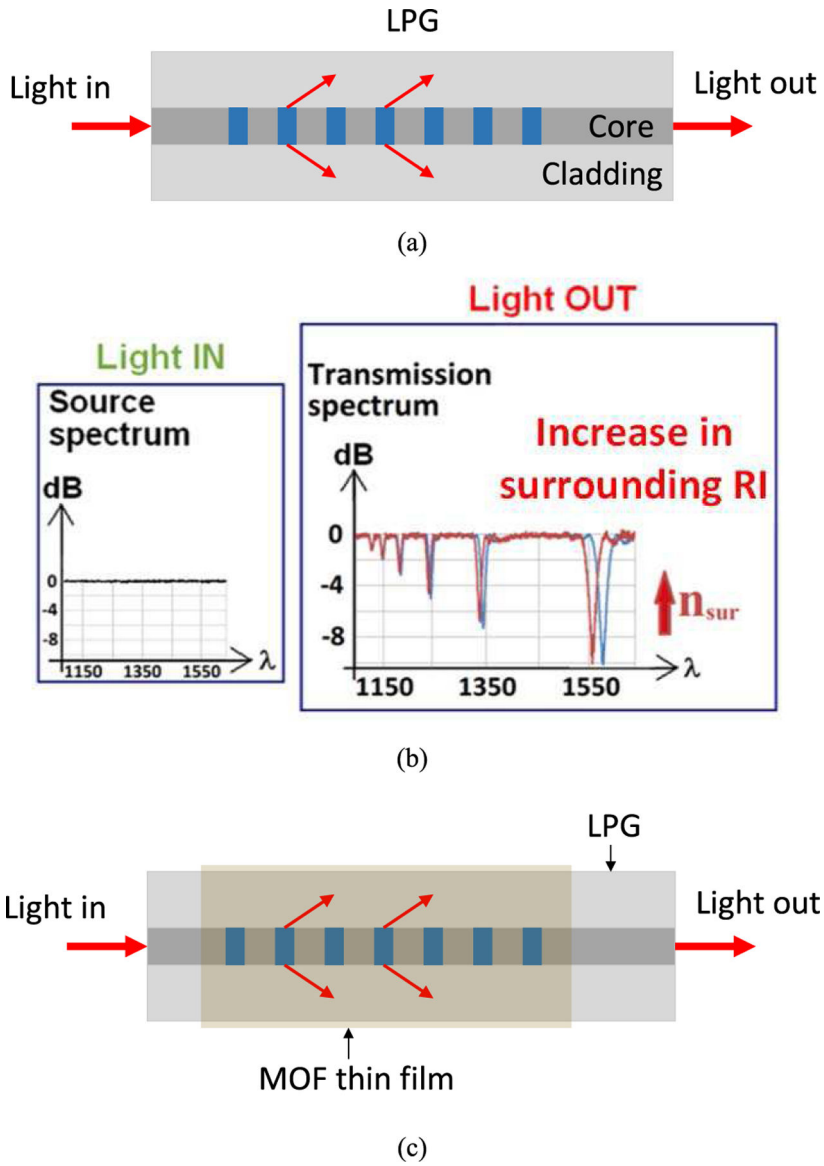

Fig. 8.

LPG chemical sensors. (a) Schematic drawing of an LPG. (b) Illustration of the response of an LPG to an increase in the RI of its surroundings. Reprinted with permission from [34]. Copyright (2015) American Chemical Society. (c) Schematic drawing of a MOF-coated LPG chemical sensor.

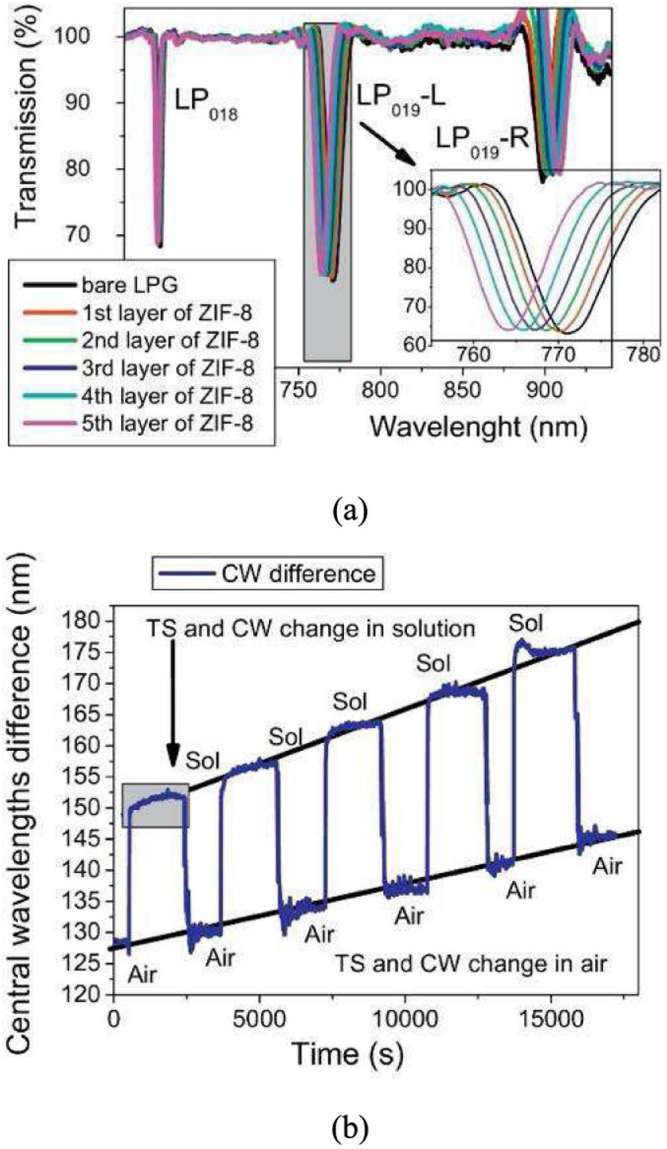

Fig. 9.

Responses of an LPG for increasing thicknesses of ZIF-8 coated on its surface. Reprinted with permission from [38]. Copyright (1969) Elsevier. (a) Transmission spectra (TS) of an LPG following the addition of sequential layers of ZIF-8. Inset shows an expanded view of the evolution of the LP_{019}-L attenuation band. (b) Dynamic shift of the central wavelength (CW) difference between LP_{019}-R and LP_{019}-L during the deposition process of the 1^{st} through the 5^{th} growth cycle. The black lines are used to guide the eye and demonstrate that the wavelength difference increased as thicker films of ZIF-8 were deposited on the fiber.

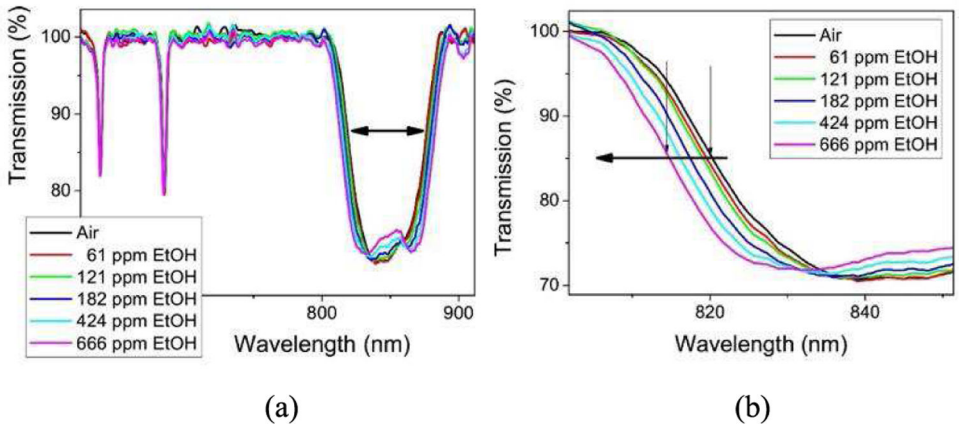

Fig. 10.

Responses of a ZIF-8 coated TAP-LPG to ethanol vapor. Reprinted with permission from [39]. Copyright (1969) Elsevier. (a) Transmission spectra of a TAP-LPG for different concentrations of ethanol. (b) Expanded view of the left section of the U-shaped attenuation band.

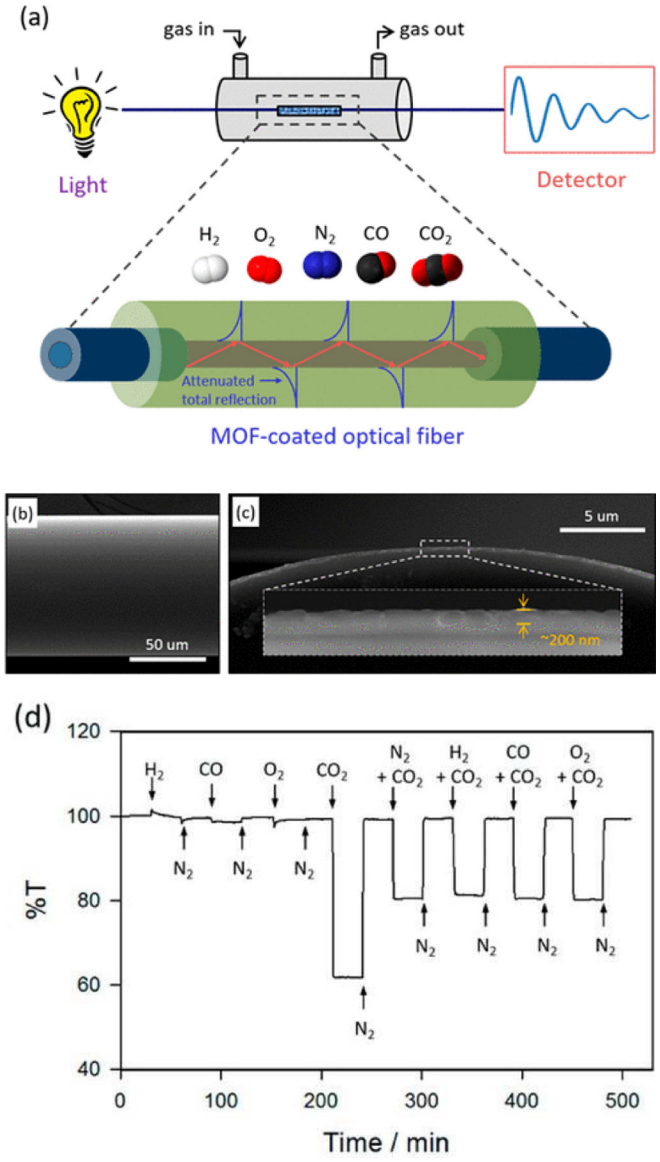

Fig. 11.

OF-MOF sensor based on an etched OF. Reprinted with permission from [16]. Copyright (2018) American Chemical Society. (a) Schematic illustration of the apparatus used to characterize the sensor. (b) SEM image of the top view of the OF-MOF sensor. (b) SEM image of the cross-section view of the OF-MOF sensor showing a 200 nm-thick ZIF-8 film coated on the outer cylindrical surface of the fiber. (d) Measured responses of a prototype sensor with a 350 nm-thick ZIF-8 layer to different gases. The transmission was measured at a wavelength of ~242 nm. N_2 was used as the reference (100% transmission) and/or carrier gas (50/50%). The experiment was performed at room temperature and 1 bar without pretreatments (e.g., heating or evacuating the ZIF-8 layer under vacuum).

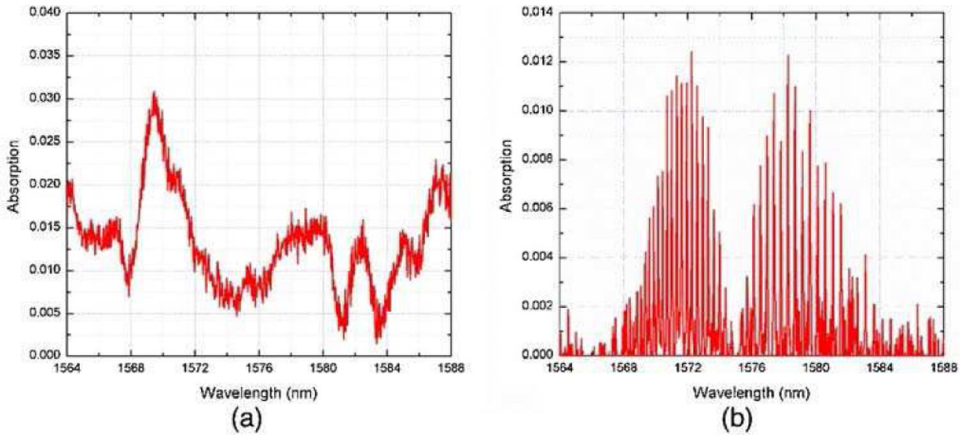

Fig. 12.

NIR absorption spectra of (a) CO_2 adsorbed inside Cu-BTC and (b) gas-phase CO_2 inside quartz gas cell. Reprinted with permission from [51]. Copyright (2016) Elsevier B.V.

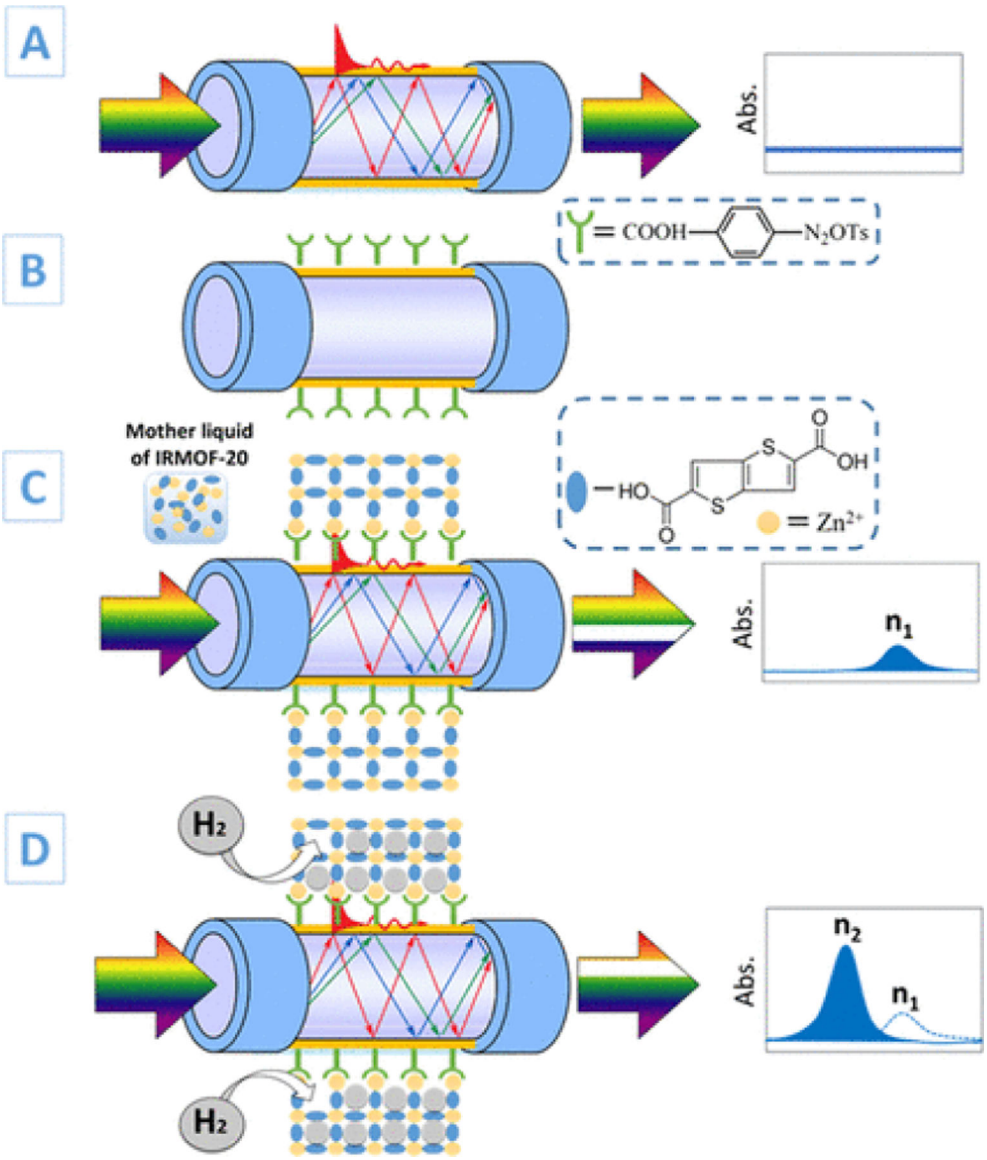

Fig. 13.

Schematic illustration of the fabrication process and working principle of the plasmonic OF-MOF hydrogen sensor. Reprinted with permission from [55]. Copyright (2019) American Chemical Society.

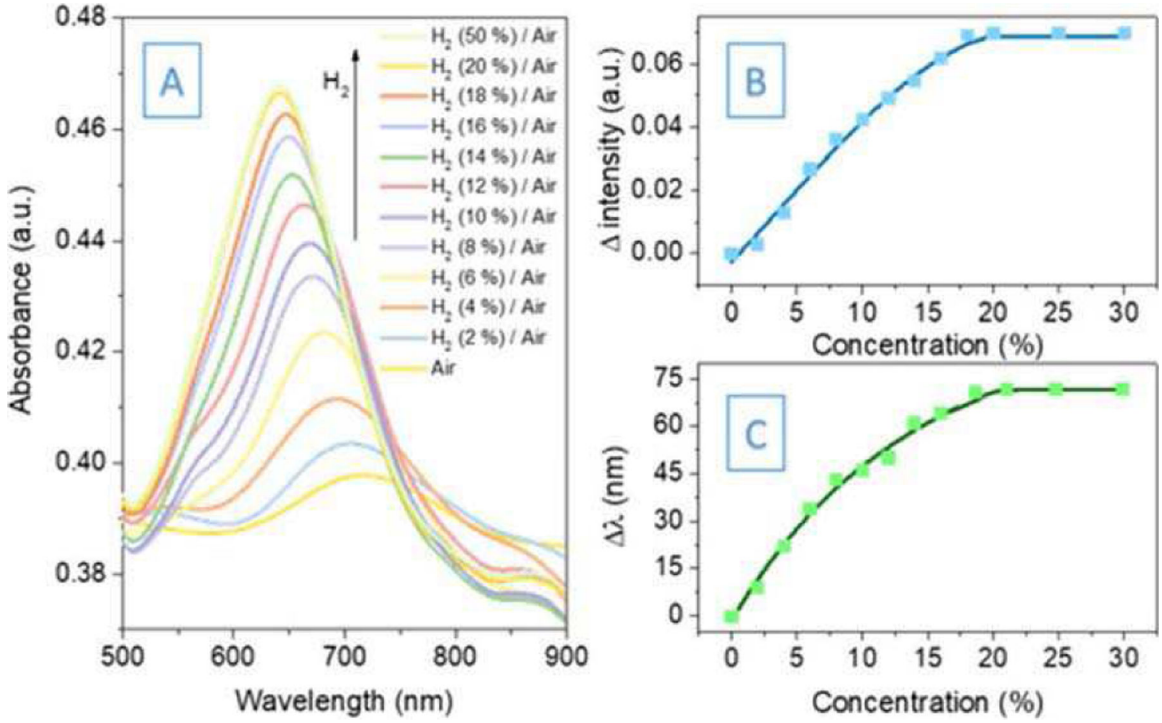

Fig. 14.

Spectroscopic characterization and performance data obtained from a plasmonic OF-MOF hydrogen sensor. Reprinted with permission from [55]. Copyright (2019) American Chemical Society. (a) Spectroscopic plasmonic adsorption bands of the sensor for different concentrations of hydrogen in hydrogen/air mixture. (b) Resonance intensity as a function of hydrogen concentration. (c) Resonance wavelength shifts as a function of hydrogen concentration.

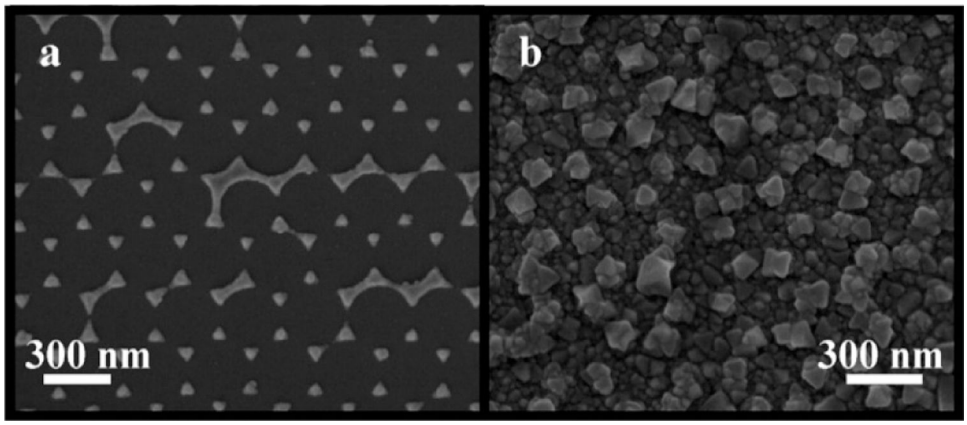

Fig. 15.

SEM images of an LSPR-MOF sensor. Reprinted with permission from [57]. Copyright (2010) American Chemical Society. (a) SEM image of a triangular Ag NP array on a glass coverslip. (b) SEM image of an HKUST-1 film coated on a NP array after 20 cycles of film growth.